The formation of Uranus and Neptune among Jupiter and Saturn

E. W. Thommes

Astronomy Department, University of California, Berkeley, CA 94720

ethommes@astro.berkeley.edu

M. J. Duncan

Physics Department, Queen's University, Kingston, Ontario K7L 3N6

duncan@astro.queensu.ca

H. F. Levison

Southwest Research Institute, Boulder, CO 80302

hal@gort.boulder.swri.edu

Received _____; accepted _____

Submitted to AJ

ABSTRACT

The outer giant planets, Uranus and Neptune, pose a challenge to theories of planet formation. They exist in a region of the Solar System where long dynamical timescales and a low primordial density of material would have conspired to make the formation of such large bodies ($\sim$ 15 and 17 times as massive as the Earth, respectively) very difficult. Previously, we proposed a model which addresses this problem: Instead of forming in the trans-Saturnian region, Uranus and Neptune underwent most of their growth among proto-Jupiter and -Saturn, were scattered outward when Jupiter acquired its massive gas envelope, and subsequently evolved toward their present orbits. We present the results of additional numerical simulations, which further demonstrate that the model readily produces analogues to our Solar System for a wide range of initial conditions. We also find that this mechanism may partly account for the high orbital inclinations observed in the Kuiper belt.

Subject headings: celestial mechanics—solar system: formation—Kuiper belt—planets and satellites: formation

1. Introduction

The growth of Uranus and Neptune in the outer Solar System is not readily accounted for by conventional models of planet formation. A low primordial density of planetesimals and weak solar gravity would have made the process of accretion slow and inefficient. In direct N-body simulations of accretion among (approximately) Earth-mass bodies beyond 10 AU, performed with three different computer codes, little accretion is found to take place over timescales of 10^8 years, and by extrapolation, over the age of the Solar System (Levison

& Stewart 2001). Earlier simulations by Brunini & Fernandez (1999) showed accretion of the ice giants in several $\times 10^7$ years with the same initial conditions, but later simulations, performed with an improved integrator, require that bodies be enhanced in radius by at least a factor of ten, relative to bodies having the density of Uranus and Neptune, in order to recover the previous result (Brunini 2000). Therefore, Uranus and Neptune are unlikely to have formed from a late stage of mergers among large protoplanets, analogous to the putative final phase of planet formation in the terrestrial zone (eg. Wetherill 1996, Chambers & Wetherill 1998). The oligarchic growth model, in which the principal growth mode is accretion of small planetesimals by a protoplanet, also produces timescales which are too long (Kokubo and Ida 2000, Thommes 2000), unless the feeding zones of Uranus and Neptune can be replenished quickly enough with low random velocity planetesimals from elsewhere in the nebula (Bryden, Lin and Ida 2000).

Thommes, Duncan & Levison (1999), hereafter TDL99, develop an alternative model to in-situ formation for the origin of Uranus and Neptune. Beginning with four or more planetary embryos of 10-15 $M_\oplus$ in the Jupiter-Saturn region, they explore through N-body simulation the evolution of the system after one of these bodies (and in one case, two at the same time) accretes a massive gas envelope to become a gas giant. They find that the remaining giant protoplanets are predominantly scattered outward. Dynamical friction with the planetesimal disk subsequently recircularizes their orbits, which leads, in about half the simulations performed, to a configuration quite similar to the present outer Solar System, with the scattered giant protoplanets taking the roles of Uranus, Neptune and Saturn. These results suggest that Uranus and Neptune are actually potential gas giant cores which formed in the same region as Jupiter and Saturn, but lost the race to reach runaway gas accretion.

Here, we explore this model in more detail, and perform further simulations. Sections

2 and 3 motivate our choice of initial conditions for the simulations. Section 4 discusses the mechanism for transporting a proto-Uranus and -Neptune to the outer Solar System. N-body simulation results are presented in Section 5. The effect on the asteroid and Kuiper belts is discussed in Section 6. We summarize and discuss our findings in Section 7.

2. Available material in the Jupiter-Saturn region

Hayashi (1981) estimated the minimum primordial surface density of solids in the outer Solar System to be

$$\sigma_{min}(a) = 2.7(a/5\,AU)^{-3/2}\,g/cm^2. \quad (1)$$

The requirement that Jupiter and Saturn's cores be massive enough to have initiated runaway gas accretion suggests that they are $\sim$ 10 $M_\oplus$ in mass (Mizuno et al 1978, Pollack et al 1996). Interior models are consistent with such a core mass, but also allow a coreless Jupiter (Guillot 1999). We assume in this work that both Jupiter and Saturn began as $\sim$ 10 $M_\oplus$ bodies; putting gas giant cores and ice giant cores on the same footing is necessary in the "strong" version of our model, though it is not essential to the basic mechanism; we discuss variations on the model in Section 7.

A surface density of 2.7 g/cm^2 was likely too low to form a $\sim$ 10 $M_\oplus$ body at 5 AU before the gas was removed from the protoplanetary disk. Lissauer (1987) finds that a surface density of 15-30 g/cm^2 is needed to allow formation of Jupiter's core on a timescale of $5 \times 10^5 - 10^6$ years, while the model of Pollack et al (1996), which includes concurrent accretion of solids and gas, produces Jupiter in less than 10^7 years with 10 g/cm^2. The formation of giant planet cores may have been triggered at least in part by the enhancement in the solids surface density beyond the "snow line", where water goes from being a gaseous

to a solid constituent of the protoplanetary disk. In fact, outward diffusion and subsequent freezing of water vapor from the inner Solar System may have resulted in a large local density enhancement around 5 AU, perhaps yielding a surface density even higher than 30 g/cm^2 (Stevenson & Lunine 1988). Here we assume a power law surface density,

$$\sigma(a) = \sigma_0 (a/5\,AU)^{-\alpha}. \tag{2}$$

The above discussion suggests $\sigma \sim 10$ to 30 g/cm^2 as a plausible surface density at 5 AU. Allowing, also, the exponent α to vary between 1 and 2, one obtains a total mass in the Jupiter-Saturn (J-S) region in excess of 40 $M_\oplus$, and as high as 180 $M_\oplus$. Therefore, it is likely that the region originally contained significantly more solids than ended up in the cores of Jupiter and Saturn.

3. Implications of oligarchic growth

Runaway growth (eg. Wetherill & Stewart 1989, Kokubo & Ida 1996) transitions to a slower, self-limiting mode called "oligarchic growth" (Ida & Makino 1993, Kokubo & Ida 1998, 2000) when the largest protoplanets are still orders of magnitude less than an Earth mass everywhere in the nebula. Oligarchic growth has previously only been demonstrated to take place interior to about 3 AU (Weidenschilling & Davis 2000). Though Kokubo and Ida make estimates of protoplanet mass and growth timescales in the giant planet region, they point out that since their simulations are restricted to annuli which are narrow compared to their radii, they cannot make strong predictions about how oligarchic growth works over a wide range in semimajor axis (Kokubo and Ida 2000). However, their most recent simulations (Kokubo & Ida 2000b) span a range of 0.5 to 1.5 AU, and show oligarchic growth proceeding in an outward-expanding "wave" over time. Also, Thommes (2000) and Thommes, Duncan & Levison (2002, preprint) perform numerical simulations which suggest that oligarchic growth does take place in the outer Solar System, and proceeds on

approximately the timescales predicted using the approach of Kokubo & Ida (2000).

Assuming that protoplanets remain approximately evenly spaced in Hill radii r_H ($1\,r_H = (M/3M_\odot)^{1/3}a$) while growing—as is characteristic of oligarchic growth—their final mass is given by

$$M = (2\pi)^{3/2}\left(\frac{2}{3M_\odot}\right)^{1/2} p^{3/2}n^{3/2}\sigma^{3/2}a^3 \tag{3}$$

where a is the protoplanet semimajor axis, n is the spacing between adjacent protoplanets in units of r_H, and p is the fraction of the total mass in the zone $[a - nr_H/2, a + nr_H/2]$ incorporated into the protoplanet (Kokubo and Ida 2000). Using numerical simulations, Kokubo & Ida (1998) show that $n \sim 5 - 10$. Models of giant planet formation by concurrent planetesimal and gas accretion suggest a surface density profile $\sigma \propto a^{-2}$ (Pollack et et 1996). Using this in Eq. 3, one obtains a protoplanet mass independent of semimajor axis. Adopting $\sigma_0 = 10\,g/cm^2$ and a spacing of n=7.5 Hill radii, one must then set the accreted mass fraction to about 0.8 in order to obtain a protoplanet mass of 10 $M_\oplus$. With this spacing, between three and five such bodies fit between 5 and 10 AU. It is likely, therefore, that this region originally contained more than just the future solid cores of Jupiter and Saturn. At the same time, the more recent simulations of Thommes, Duncan and Levison (2002) indicate that accretion is quite inefficient in the outer Solar System; even in the Jupiter-Saturn region, the above value of p is probably overly optimistic, and a correspondingly higher density of solids in this region may have been necessary to form gas giant cores. But as we find (Section 5.5), a higher-density disk actually tends to increase the "success rate" of the model.

4. Scattering and circularization of the protoplanets

In the nucleated instability picture of gas giant formation, there are three distinct phases of growth (Pollack et al 1996): In Phase 1 (which itself encompasses the sub-phases

of runaway and oligarchic growth; see Section 3 above), a solid core grows until it depletes most of the material in its feeding zone. Phase 2 is characterized by much slower growth, with gas accretion gradually coming to dominate over solids accretion. After a time of order several Myrs, the protoplanet contains comparable masses of gas and solids; around this time, the third phase of runaway gas accretion sets in and proceeds on a timescale of $\sim 10^5$ years. One of the protoplanets in the Jupiter-Saturn region must have been the first to reach this point. Shorter formation timescales at smaller heliocentric radii argue for Jupiter having formed before Saturn. The relatively long time spent by a protoplanet on the "plateau" of Phase 2 means that several protoplanets could plausibly find themselves there by the time the first of them makes it to Phase 3. Furthermore, if the winner has a broad enough margin of victory, its rivals will have only had time to accumulate a few $M_\oplus$ of gas, thus resembling the present-day ice giants in both solids and gas mass.

A body increasing its mass from 10 $M_\oplus$ to Jupiter's mass, $M_J = 314\ M_\oplus$, expands its Hill radius by a factor of about three. The adjacent protoplanets will therefore have a high likelihood of being gravitationally scattered. In a three-body system—Sun, Jupiter and a single protoplanet—a Jupiter-crossing protoplanet would continue to have close encounters with its much more massive scatterer, and so would remain coupled to it, unless it were scattered onto an unbound orbit and left the system altogether. In reality, however, one expects that as it crosses beyond the Jupiter-Saturn region, a body will encounter a less accretionally evolved part of the protoplanetary disk, consisting predominantly of much smaller bodies. As a result, the protoplanet will experience dynamical friction. This will tend to reduce the eccentricity of its orbit. If the eccentricity decays enough, the protoplanet's perihelion will be lifted away from Jupiter, thus decoupling it from its scatterer. Insofar as one can neglect interactions with other scattered protoplanets, its eccentricity will then monotonically decrease until it reaches equilibrium with the planetesimals. The eccentricity rate of change due to dynamical friction on a body of mass

M in a swarm of mass m bodies can be expressed as (Weidenschilling et al 1997)

$$\frac{de_M^2}{dt} = C(m\langle e_m^2\rangle - Me_M^2)K_e \tag{4}$$

and a similar expression gives the time evolution of the inclination. $\langle e_m^2\rangle^{1/2}$ is the RMS eccentricity of the mass m bodies, and K_e is a definite integral depending on the inclinations and eccentricities, defined in Stewart & Wetherill (1988). The coefficient C is given by

$$C = \frac{16G^2\rho_{sw1}ln\Lambda}{v_K^3(\langle e_1^2\rangle + \langle e_2^2\rangle)^{3/2}}, \tag{5}$$

where G is the gravitational constant, v_K the local Keplerian velocity, ρ_{sw1} the spatial mass density of the swarm, and Λ is approximately the ratio of the maximum encounter distance between the body M and a member of the population of the swarm, to the maximum separation that results in a physical encounter (Stewart & Wetherill 1988).

An equilibrium is therefore reached when

$$e_M^2 M \simeq \langle e_m^2\rangle m \tag{6}$$

This also means that as long as

$$e_M^2 M \gg \langle e_m^2\rangle m, \tag{7}$$

the eccentricity decay rate of the body M will only depend on the spatial mass density of the planetesimal disk, and will be essentially independent of the individual masses of the planetesimals. This feature will be exploited in the numerical simulations below. One can estimate the time for the eccentricity to be reduced by half as

$$T_{df_{e/2}} \sim \left|\frac{e_{M0}/2}{de_{M0}/dt}\right| = \left|\frac{e_{M0}^2}{de_{M0}^2/dt}\right| \tag{8}$$

Fig. 1 plots this timescale estimate for a Jupiter-crossing 10 $M_\oplus$ body, over a range in semimajor axis. The planetesimal disk parameters used are those for the baseline simulation below (Section 5.1). As can be seen, the eccentricity-halving timescale reaches $\sim$ 2 Myrs, or just over 10^4 orbital periods, at the outer edge of the present-day giant planet region (30 AU)

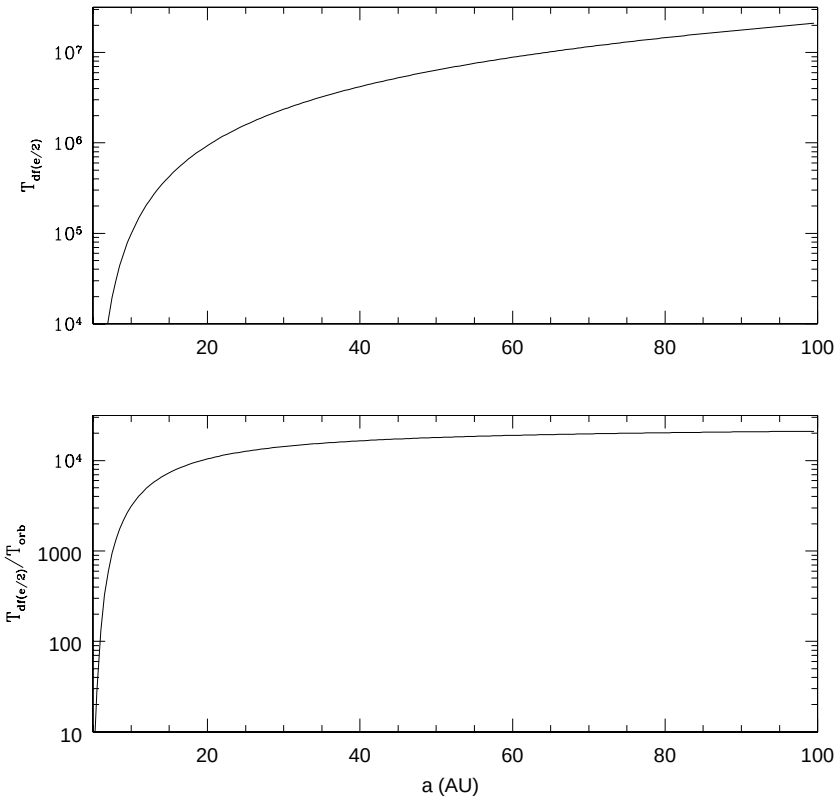

Fig. 1.— A (rough) approximation of the eccentricity-halving timescale due to dynamical friction, $T_{df\,e/2}$, for a 10 $M_\oplus$ body in the outer Solar System having an initial eccentricity such that it is Jupiter-crossing, with its pericenter at 5 AU ($e_0 = 1 - (5AU)/a$). The top panel plots the time in years, while the bottom panel plots it in units of the local orbital period. The planetesimal disk is taken to have a surface density of $\sigma(r) = 10(r/5\text{ AU})^{-2}\text{g/cm}^2$, an RMS eccentricity $e_m = 0.05$, and a thickness $2h \sim 2ai_m \sim ae_m$. $\ln(\Lambda)$ is given a typical value of 3 (eg. Kokubo & Ida 2000). In computing $T_{df\,e/2}$, we approximate the effective surface density of planetesimals encountered on an orbit with semimajor axis a as $\sigma(a)$, regardless of the orbit's eccentricity.

5. N-body simulations

Putting the pieces together, one can now envision a scenario in which a) a rapidly growing Jupiter scatters its smaller neigbours outward, and b) these "failed cores" are decoupled from Jupiter and ultimately evolve onto circular, low-inclination orbits in the outer Solar System. TDL99 performed three series of numerical simulations to test this model; about half of the simulations produced a stable final configuration qualitatively similar to the present-day Solar System. Here, we expand on the earlier work, performing simulations to assess the effect of other planetesimal disk density profiles and of proto-Jupiter being initially not the innermost giant protoplanet. We also investigate how sensitive this scenario is to the timing of Saturn's final stage of growth, relative to that of Jupiter. Simulations are once again performed using the proven SyMBA symplectic integrator (Duncan, Levison & Lee 1998). This integrator is able to handle close encounters among massive bodies while preserving the symplectic properties of the method of Wisdom & Holman (1991).

5.1. Initial conditions: Set 1

For the baseline set of simulations, a planetesimal disk of surface density

$$\sigma_1 = 10(a/5\,AU)^{-2}\ g/cm^2 \tag{9}$$

is used, with the disk extending from 5 to 60 AU. The above density profile is steeper than those of TDL99 ($\sigma \propto a^{-1}$ and $a^{-3/2}$). The total disk mass between 10 and 60 AU (106 $M_\oplus$) is about half that of the first two sets of runs in our earlier work (216 $M_\oplus$), and similar to that in the third run (119 $M_\oplus$). The truncation at 60 AU is to keep the number of bodies in the simulations tractably small; in reality the planetesimal disk may have extended for hundreds of AU, far beyond the presently visible Kuiper belt. Observational evidence does

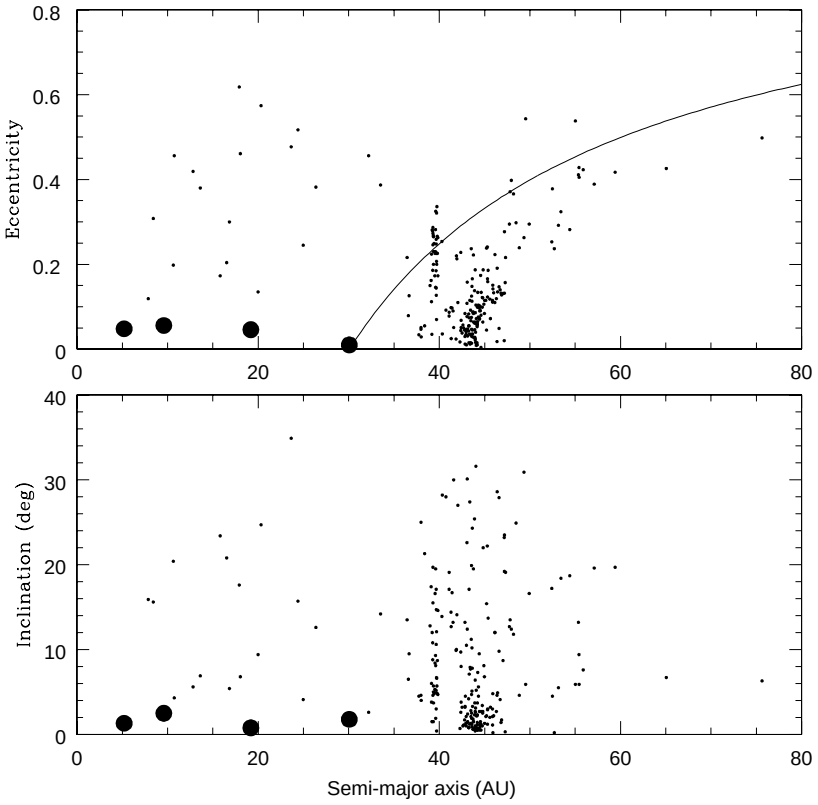

Fig. 2.— Eccentricities (top) and inclinations (bottom) in the outer Solar System at the present epoch, showing the giant planets as well as all Kuiper belt objects and Centaurs (objects with a . 30 AU) which have been observed at multiple oppositions, as of September 2001. The curve in the top panel shows the locus of orbits with perihelia at the semimajor axis of Neptune. KBO and Centaur data is taken from the Minor Planet Center site, cfa-www.harvard.edu/iau/mpc.html

point to the possibility of a truncation of the belt at $\sim$ 50 AU (eg. Chiang & Brown 1999). But if a "Kuiper cliff" exists, it is not necessarily primordial.

Since we truncate the disk at a location where the planetesimal surface density is already very low (0.07 g/cm^2 for the density profile of Eq. 9), one expects this not to have a strong effect on the evolution of any scattered protoplanets which cross the region $r > 60$ AU. As a test, we perform four pairs of runs comparing the evolution of a 10 $M_\oplus$ body with initial $a = 100$ AU, $e = 0.9 - 0.95$ in planetesimal disks with a surface density as prescribed by Eq. 9, in one case extending to 60 AU, in the other to 200 AU. No systematic difference in the 10 $M_\oplus$ body's semimajor axis evolution over the first few Myrs is apparent between the two different disk sizes. The eccentricity, however, tends to be damped more rapidly in a 200 AU disk. We expect, therefore, that the subsequent runs somewhat underestimate the effectiveness with which those scattered protoplanets which cross beyond 60 AU are circularized, if the disk was in fact larger. In particular, a planetesimal disk with a radius of hundreds of AU may allow the retention of protoplanets which in our runs are scattered strongly enough to become unbound; we will explore this possibility in future work.

The simulated disk is made up of equal-mass "planetesimals", each having a mass of 0.2 $M_\oplus$. At twice the mass of Mars, these bodies far exceed the actual characteristic mass of planetesimals in the early outer Solar System. In reality planetesimals are thought to have been on the order of 1 to 100 km in size, thus with a mass of $\sim 10^{-12} - 10^{-6}$ $M_\oplus$ (eg. Lissauer 1987). The unrealistically large masses are chosen to keep the number of bodies manageably low, at slightly over 500. As mentioned in Section 4, when the large bodies have eccentricities high enough that Eq. 7 is satisfied, the eccentricity decay timescale will be effectively independent of the planetesimal masses. Thus despite the large planetesimal masses, the initial strength of eccentricity damping will be realistic. The equilibrium eccentricity condition Eq. 6, however, does depend on the planetesimal mass, so the

equilibrium eccentricity reached by a large body among the planetesimals in the simulation will tend to be unrealistically high. Of course, a true equilibrium between protoplanets and planetesimals will not exist anyway, since mutual perturbations among the protoplanets will also have an effect.

The initial planetesimal eccentricities and inclinations are given a Rayleigh distribution in e and i, (Kokubo and Ida 1992) with $\langle e^2 \rangle^{1/2} = 0.05$, $\langle i^2 \rangle^{1/2} = 0.025 = 1.4^o$. In the numerical integrations, the planetesimals are treated as a "second-class", non-self-interacting population. Thus they are perturbed in their Keplerian orbits only by forces from the protoplanets, not each other. The protoplanets, on the other hand, are subject to forces from each other as well as from the planetesimals. This serves two purposes: It makes the simulations run much faster, since for N second-class bodies, the computation time scales as N instead of N^2. Also, it prevents unrealistically strong self-stirring of the disk. Of course, not modeling planetesimal interactions means that collective planetesimal effects are not accounted for. Wave phenomena could have had an important effect on the evolution of the planetesimal disk velocity distribution (eg. Ward and Hahn 1998), provided the disk was sufficiently massive and dynamically cold. However, it is unlikely that significant wave phenomena could persist once the initial scattering has taken place and the planetesimal disk has been stirred by eccentric 10 $M_\oplus$ bodies.

Also unmodeled is nebular gas, either as a source of aerodynamic drag (relevant for small planetesimals; eg. Adachi, Hayashi and Nakazawa 1976), or as a source of tidal forces (relevant for bodies & 0.1 $M_\oplus$; eg. Ward 1997). The former mechanism will keep the planetesimal disk more dynamically cold, but this does not affect the strength of dynamical friction on larger bodies until $e_M^2 M \sim e_m^2 m$. The latter effect is thought to cause the inward migration of $\sim$ 1 - 10 $M_\oplus$ objects on timescales short compared to their formation times. This of course constitutes a potentially severe problem not only for our model, but for

any model of giant planet formation which requires the accumulation of large solid cores. Addressing this problem is beyond the scope of our present work, but we summarize some reasons why it may in reality have been less severe, in Section 7.

The 10 $M_\oplus$ bodies are given a density $\rho = 0.25\rho_\oplus = 1.5$ g/cm^3, roughly equal to that of Uranus and Neptune. This gives them radii of 2.18×10^4 km. Four such bodies are put in the simulation, initially on nearly circular and uninclined orbits. The orbits are spaced by 7.5 mutual Hill radii, starting from an innermost distance of 6 AU to allow for later inward migration by Jupiter. Thus the bodies' initial semimajor axes are 6.0 AU, 7.4 AU, 9.0 AU and 11.1 AU. Between 5 and 12 AU, the disk is depleted in planetesimals so that the surface density is still given by Eq. 9. Since the large bodies are spaced proportionally to their semimajor axes, their distribution is consistent with a surface density $\propto a^{-2}$.

Integrating the surface density from 5 to 12 AU, the total mass is 51.5 $M_\oplus$. With 40 $M_\oplus$ of this in the large bodies, this leaves 10.5 $M_\oplus$ in planetesimals in the Jupiter-Saturn region, in addition to 94.7 $M_\oplus$ between 12 AU, and the outer disk edge at 60 AU. In summary, then, the initial conditions amount to a state where Phase 2 of giant planet formation has been reached between 5 and 12 AU, with $\sim 80\%$ of the planetesimals having accreted through oligarchic growth into four bodies of 10 $M_\oplus$ each, while no large bodies have yet formed beyond this region (Fig. 3). The adoption of equal-mass protoplanets is a simplification; apart from stochastic variations among the oligarchic growth endproducts, one can expect some intermediate bodies, with masses perhaps up to a few $M_\oplus$. Such bodies are likely to ultimately be cleared, along with the planetesimals, from the giant planet region. However, they may end up playing a role in the dynamics of the trans-Neptunian region; see Petit, Morbidelli and Valsecchi (1999).

For computational reasons, the inner simulation radius is chosen as 1 AU; any body whose orbit penetrates this boundary is eliminated from the system. This is done because

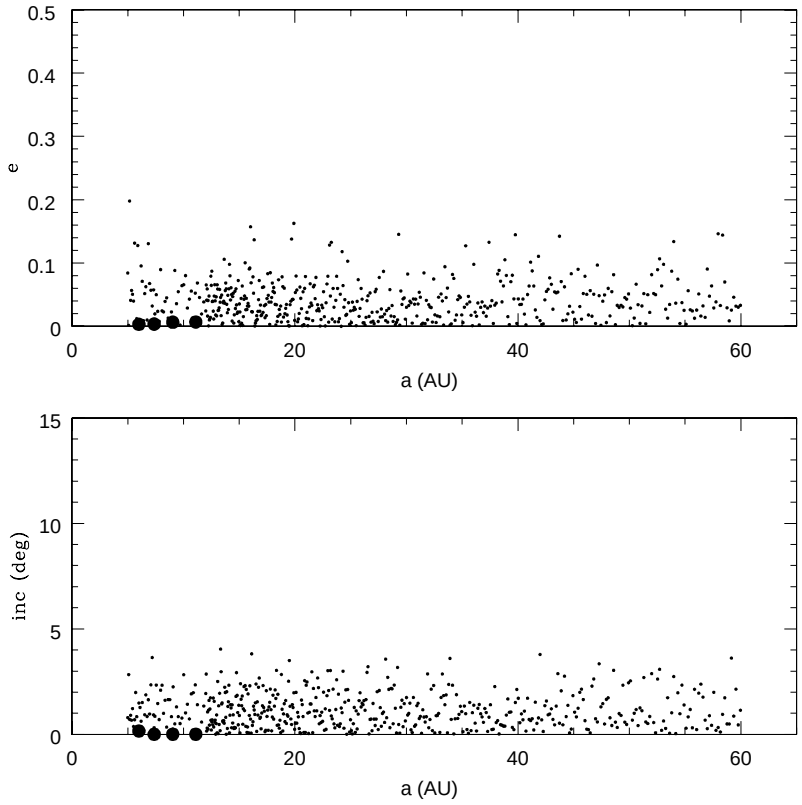

Fig. 3.— Initial state for runs in Set 1, showing eccentricity (top) and inclination (bottom) versus semimajor axis. The larger circles denote the four 10 $M_\oplus$ protoplanets, and each of the small dots represents a 0.2 $M_\oplus$ planetesimal. The planetesimal density in the vicinity of the protoplanets is decreased to keep the density of protoplanets plus planetesimals consistent with the surface density given by Eq. 9.

a limitation of the SyMBA integrator used here is its inability to handle close perihelion passages. Although a new version of SyMBA has since been developed which removes this restriction (Levison and Duncan 2000), the runs presented here predate this development. In any case, this limitation has little relevance for the present runs; typically, less than ten planetesimals are lost at the inner boundary over the course of a 5 Myr simulation. The base timestep is chosen as 0.05 years, giving 20 steps per orbital period for an orbit with its semimajor axis at the inner radius, and over 200 steps per orbit for Jupiter. Experimentation shows that this timestep is small enough that the energy of the system is well-conserved. Runs initially go to 5 Myrs; in cases where the system still appears to be undergoing rapid evolution at this point, the runs are extended by another 5 Myrs.

5.2. Set 1 results

To model gas accretion, SyMBA was modified to allow a subset of bodies to have artificially time-varying masses (in addition to any changes in mass resulting from the accretion of other bodies). For the runs in Subset 1, it is assumed that the innermost protoplanet undergoes runaway gas accretion first, and grows into Jupiter. The simulations start at the time when this happens, which should be a few million years into the life of the solar system (see Section 3 above). Runaway gas accretion is simulated by increasing the body's mass over the first 10^5 years of simulation time, from its original mass of 10 $M_\oplus$ to 314 $M_\oplus$, approximately the present Jupiter mass. A linear growth in mass is used; this is deemed appropriate since the actual time evolution of mass during runaway growth is highly uncertain. Also, as the simulations will show, 10^5 years is roughly the response time of the system, and the system's subsequent evolution is therefore unlikely to be affected in a systematic way by the exact form of the time evolution of the runaway-phase mass growth.

Set 1 consists of eight alternate realizations of a run, differing only in the initial phases

of the four protoplanets; for each, the angles Ω, ω and M are randomly generated. As will be seen, the stochasticity of the system ensures that this difference in phases is sufficient to bring about a very different evolution in each of the versions of the run.

Fig. 4 shows the evolution of one of the eight runs, denoted as Run 1F, which after 5 Myrs produces final protoplanet orbits that bear a particularly close resemblance to those of the giant planets in the present-day Solar System. Semimajor axis, perihelion distance and aphelion distance are plotted versus time for each of the four protoplanets; the innermost one has grown into Jupiter after the first 10^5 years. By this time, the protoplanet orbits begin to mutually cross, and strong scattering occurs. The protoplanet plotted in red briefly has its semimajor axis increased to greater than 100 AU. However, dynamical friction acts to reduce eccentricities universally, decoupling the protoplanets from Jupiter and from each other. By about 1.2 Myrs, none of the protoplanets are on crossing orbits anymore. After about 3 Myrs, the bodies no longer undergo any changes in semimajor axis greater than a few AU on a million-year timescale. At this point the orbits are well spaced and all eccentricities are $\lesssim 0.05$, with no large fluctuations. Due to the large stochastic variations among runs, the exact timescales differ, but we find that orbits typically become noncrossing after less than 5 Myrs in these and subsequent runs. This is consistent with Fig. 1, which predicts timescales on the order of Myrs for the circularization of bodies scattered into the outer Solar System.

Subsequent semimajor axis evolution proceeds by scattering of planetesimals by protoplanets, rather than scattering of the protoplanets off each other and Jupiter. As planetesimals are scattered among Jupiter and the protoplanets, the former experiences a net loss of angular momentum while the latter experience a gain. Thus Jupiter's orbit shrinks, while those of the protoplanets expand (Fernandez and Ip 1996, Hahn and Malhotra 1999). This phase takes place over a timescale of several tens of Myrs and ends, at the

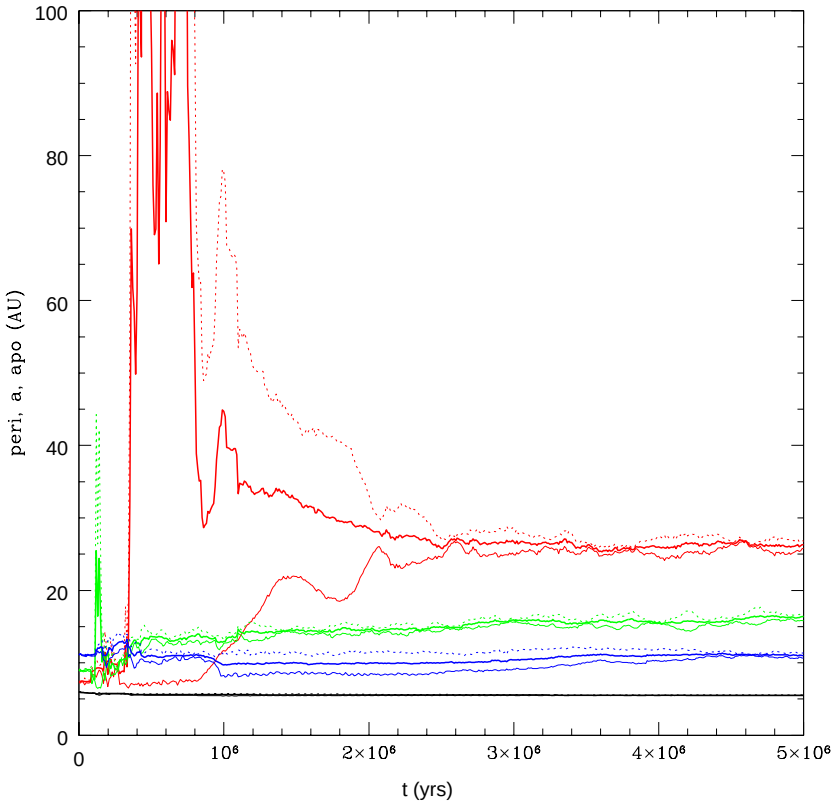

Fig. 4.— Run 1F: Evolution of semimajor axis (bold lines), perihelion distance q (thin lines) and aphelion distance Q (dotted lines) of the four 10 $M_\oplus$ protoplanets. The protoplanet which grows to Jupiter mass (314 $M_\oplus$) over the first 10^5 years of simulation time is shown in black.

very latest, when the planetesimals have been cleared from among the planets. Because the length of migration during this phase is only a few AU, and to save time, most of the runs are stopped after 5 Myrs. As an example, Fig. 5 shows Run 1F continued to 50 Myrs; the net migration of the outer two protoplanets subsequent to 5 Myrs is only $\sim$ 1 - 4 AU outward.

The semimajor axes at which the scattered bodies end up are very noteworthy, if one compares them to the present orbits of the giant planets (Fig. 2). At 5 Myrs, the outer two protoplanets are at 16 and 26 AU. The innermost one is at 11 AU, while Jupiter is at 5.5 AU. This configuration of orbits is very similar to that of the present Solar System, where Uranus and Neptune are at 19 and 30 AU respectively, Saturn is at 9.6 AU, and Jupiter is at 5.2 AU. And at 5×10^7 years, after some more net outward migration, the outer two protoplanets' semimajor axes are even closer to those of Uranus and Neptune (though "proto-Saturn", having also moved outward, is further away from its present orbit). Eccentricities and inclinations are likewise very close to their present values.

The end states of all the runs in Set 1 are summarized in Fig. 6. Depicted are snapshots of eccentricity versus semimajor axis at 5 Myrs, except for Runs 1A and 1H, which were continued to 10 Myrs. These were extended because one or more of the protoplanets still had a high but decreasing eccentricity at 5 Myrs.

Runs 1A, 1D, 1F, 1G and 1H result in a final ordering of orbits that is at the very least broadly consistent with the present Solar System: Jupiter is the innermost body, with the other three bodies interior to the region of the Kuiper belt, and eccentricities low enough that no protoplanets cross each other or Jupiter. Out of these five runs, 1D and 1F in particular resemble the present Solar System. Of course, to actually reproduce the Solar System, another important event has to take place: The next protoplanet beyond Jupiter must also undergo a runaway gas accretion phase to acquire an envelope of mass

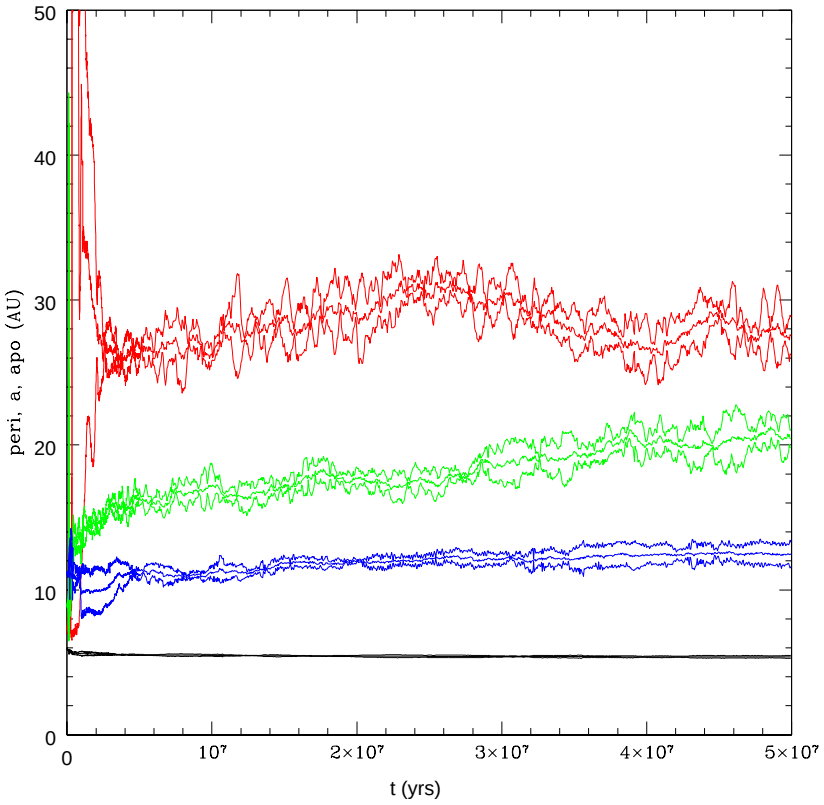

Fig. 5.— Run 1F continued to 50 Myrs. Between 5 Myrs and 50 Myrs, the net migration for Jupiter and the protoplanets, going from inside to outside in semimajor axis, is -0.2 AU, 1.5 AU, 4 AU, and 1.3 AU.

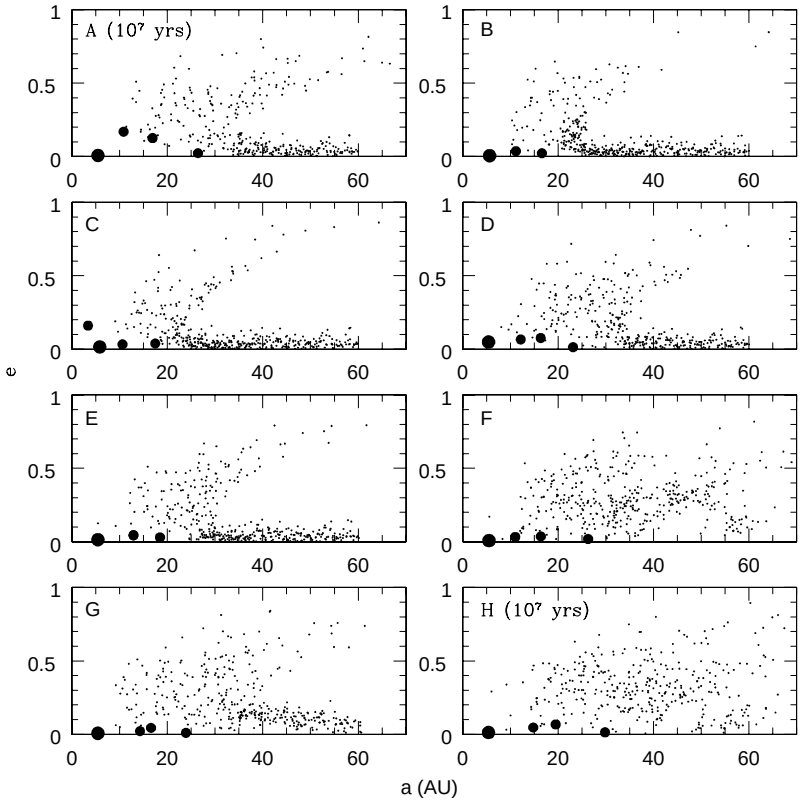

Fig. 6.— Endstates of the eight Set 1 runs, after 5 Myrs of simulation time, except for 1A and 1H, which were continued on to 10 Myrs. Eccentricity is plotted versus semimajor axis. The three different sizes of points denote planetesimals (smallest), 10 $M_\oplus$ protoplanets (medium), and Jupiter (largest). Planetesimal orbits crossing Jupiter or any of the protoplanets are generally unstable on timescales short compared to the age of the Solar System, thus the region among the protoplanets would be essentially cleared of planetesimals long before the present epoch.

& 80 $M_\oplus$ and become Saturn. With the innermost core on a stable orbit in the vicinity of Saturn's present location, though—as it is in runs 1D and 1F—the time delay between Jupiter and Saturn's runaway phases appears not be strongly constrained. A more detailed investigation of the role of Saturn's growth will follow in Section 5.8.

In contrast, Uranus and Neptune must somehow have been prevented from later reaching runaway gas accretion. One possibility is that they simply ran out of time, still caught in the long plateau of the second giant planet growth phase (Pollack et al 1996; see Section 4) when the nebular gas was removed. Alternatively, it may be that the gas disk was truncated early on by photoevaporation between the orbit of Saturn, and the eventual orbit of Uranus (Shu, Johnstone and Hollenbach 1993). This possibility is discussed further in Section 7.

The final state of the planetesimal disk differs substantially among the runs. In 1B and 1C , the planetesimal disk is largely unperturbed over most of its radial extent, while in 1F and 1H, eccentricities have been greatly increased throughout the entire disk. The rest of the runs are intermediate cases. The radial extent of the perturbation simply depends on how much of the disk is crossed by the protoplanets over the course of the run. In Run 1F, for example, Fig. 4 shows that one body's aphelion spends some time beyond 100 AU. On the other hand, in 1C, no protoplanet's aphelion ever goes further out than $Q_{max} \simeq 18$ AU. In those runs where $Q_{max} < 60$ AU (the disk radius), Q_{max} corresponds closely to where the planetesimal disk makes a transition from perturbed to unperturbed. The outer limit of the planetesimal disk's excitation by scattered protoplanets has been referred to as the "fossilized scattered disk" (TDL99). The contemporary scattered disk, by contrast, consists of objects which were scattered by Neptune after the latter had attained its current orbit (Duncan and Levison 1997). A more detailed discussion of the fossilized scattered disk follows in Section 6.2.

Previous work has shown that a slow, steady outward migration of Neptune, like that which would accompany the scattering of planetesimals among the giant planets (see above), results in the capture of planetesimals into Neptune's exterior mean-motion resonances (Malhotra 1995). One would expect the same thing to happen in the model presented here, once the giant planets are no longer strongly perturbing each other and can migrate smoothly. None of the simulations, however, show any evidence of resonant capture of planetesimals. The problem is that the exaggerated planetesimal masses make the migration too jittery for any planetesimals to be entrained in the resonances. The simulations of Hahn and Malhotra (1999) clearly show the trend of smoother migration for smaller planetesimal masses, however even with their smallest mass of 0.01 $M_\oplus$, they find no resonant capture; the disk is still too discretized. However, in our model, there is the additional feature that the planetesimal disk tends to get strongly stirred during the initial scattering of the giant protoplanets. Since the probability of a body to be resonantly captured decreases with its initial eccentricity (eg. Borderies and Goldreich 1984), the subsequent capture efficiency will be lower than if Neptune's resonances sweep through an unperturbed disk, even if Neptune's migration is perfectly smooth in both cases.

Three of the runs produce systems at 5 Myrs that are irreconcilably different from our own. In 1B, one of the protoplanets has merged with Jupiter. In 1C, a protoplanet has been scattered onto an orbit interior to Jupiter, in the region of the present-day asteroid belt, with its semimajor axis at 3.4 AU, its perihelion at 2.8 AU and its aphelion at 3.9 AU. It attains a stable orbit not crossing Jupiter even though the only planetesimals available for damping interior to Jupiter are those few which are also scattered there. This is possible because the protoplanet is scattered not just by Jupiter, but also by the other protoplanets. Even assuming the protoplanet could be subsequently removed from this region, such an event would most likely have cleared much of the asteroid belt. Finally, in 1E, two of the protoplanets have merged. It should be noted that mergers—or, indeed, ejections—which

reduce the number of protoplanets are not intrinsically a problem, since extra ones may have existed. Scenarios with five protoplanets (Jupiter + Saturn + 3) will be explored in Section 5.4.

5.3. Set 2: Dependence on initial ordering

How strongly does the final configuration of the system depend on the initial ordering of the protoplanets? The next set of runs, Set 2, uses the same initial conditions, within a random variation in the protoplanet phases, as Set 1. However, for these runs it is the second-innermost protoplanet, rather than the innermost one, which undergoes simulated runaway gas accretion. One can reasonably expect that this will favour an outcome like 1C (Fig. 6), where a protoplanet is scattered inward into the region of the asteroid belt.

The end states of the runs are shown in Fig. 7. In six of the eight runs, a protoplanet has indeed ended up interior to Jupiter. However, in two cases (2C and 2D), Jupiter is the innermost body. Thus it appears that if Jupiter does not grow from the innermost protoplanet, the likelihood of ending up with a final configuration similar to our Solar System declines, though such an outcome continues to be quite possible.

5.4. Set 3: Dependence on number of cores

How sensitively does the end state depend on the initial number of core-sized bodies? In the next set of simulations, an extra 10 $M_\oplus$ protoplanet is added. All protoplanets are more tightly spaced, by 6.5 instead of 7.5 mutual Hill radii. Starting, again, from 6.0 AU, the outermost protoplanet is therefore initially at 12.2 AU. The surface density of planetesimals in the region of the protoplanets is reduced to keep the average surface density unchanged at $\sigma_1 = 10(a/5\,\mathrm{AU})^{-2}$ g/cm^2. The innermost protoplanet is, again,

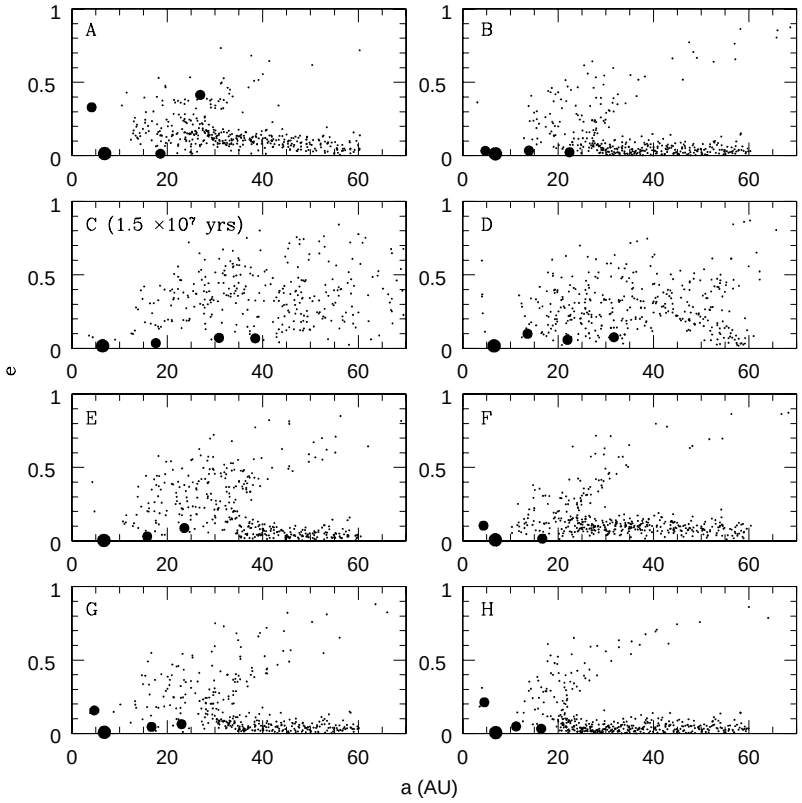

Fig. 7.— End states of the eight Set 2 runs (second-innermost protoplanet becomes Jupiter), after 5 Myrs of simulation time, except for 2C, which was continued on to 15 Myrs. Eccentricity is plotted versus semimajor axis. The three different sizes of points denote planetesimals (smallest), 10 $M_\oplus$ protoplanets (medium), and Jupiter (largest).

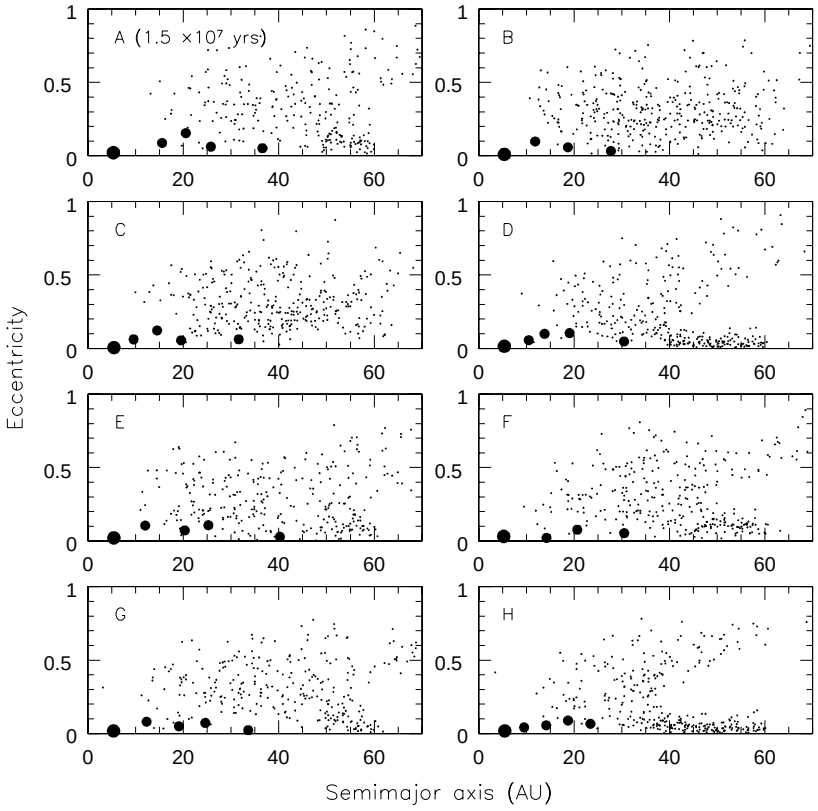

Fig. 8.— End states of the eight Set 3 runs (one extra protoplanet), after 10 Myrs of simulation time, except for 3A, which was continued on to 15 Myrs.

increased in mass to that of Jupiter over the first 10^5 years.

Fig. 8 shows the endstates of the runs. This time all runs initially have a length of 10^7 years, since the larger number of bodies take longer to decouple from each other. Run 3A is continued to 1.5×10^7 years, because after 10^7 years some of the protoplanets are still on crossing orbits. Eccentricities are uniformly low and the protoplanet orbits are well-spaced for the most part, thus the systems have a good chance of being stable indefinitely. However, once all the planetesimals have been scattered from among the protoplanets, so that the latter are no longer subject to dissipative forces, some of these systems may still become unstable. This caveat applies to all the runs presented in this work, but generally speaking, larger numbers of bodies increase the potential for instability (Levison, Lissauer and Duncan 1998).

All of the protoplanets remain in six of the eight runs, thus resulting in systems with one too many planets relative to the present Solar System. However, in Runs 3B and 3F, one of the protoplanets is ejected from the Solar System, leaving the right number of bodies behind. In both of these runs, a protoplanet ends up with a semimajor axis within 10% of present-day Uranus and Neptune, respectively, though both "Saturns" are too far out. One may conclude that with one extra initial protoplanet in the Jupiter-Saturn region, scattered protoplanets continue to be readily circularized, and the resulting systems tend to look like ours with one extra outer planet. However, a system with four giant planets remains a possible outcome. Also, the subsequent formation of Saturn from one of the protoplanets may trigger more ejections, especially in those cases where the inner protoplanets are more closely spaced, such as 3D and 3H.

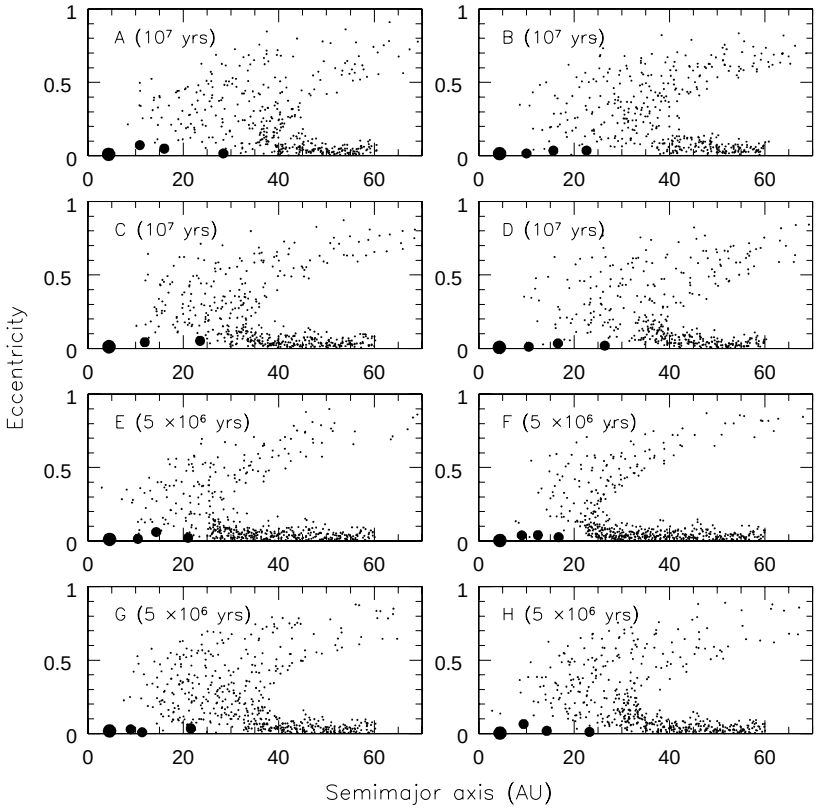

Fig. 9.— End states of the eight Set 4 runs (a more massive planetesimal disk). The first four are run to 5×10^6 years; the last four are run to 10^7 years.

5.5. Set 4: A more massive planetesimal disk

In this set of runs, a number of parameters are changed to simulate a system with a more massive planetesimals disk. The protoplanets are now 15 $M_\oplus$ bodies. The planetesimal disk surface density profile is still $\propto a^{-2}$, but it is scaled up to be 15 g/cm^2 at 5 AU; that is,

$$\sigma_2 = 15(a/5\ \mathrm{AU})^{-2}\, g/cm^2. \tag{10}$$

Other minor differences are a legacy of chronologically earlier runs. The innermost protoplanet is initially at 5.3 AU, and successive protoplanets are spaced by only 5.8 mutual Hill radii. Thus the outermost protoplanet is initially at 9.0 AU. The individual planetesimals have a mass of 0.24 $M_\oplus$.

The innermost protoplanet, as before, has its mass increased to 314 $M_\oplus$ over the first 10^5 simulation years. The end states of the runs are shown in Fig. 9. All except C yield the correct number and ordering of bodies, and eccentricities are uniformly low. This "success rate" is higher than that of Set 1, in which only five out of eight runs yield qualitatively the correct orbital configuration. This is accounted for by the more massive planetesimal disk; it provides stronger dynamical friction, so that scatterings of protoplanets tend to be less violent, and subsequently, orbits tend to be circularized and mutually decoupled more quickly. Runs A, D and H end up with protoplanet orbits that are particularly close to those of Saturn, Uranus and Neptune. Jupiter systematically ends up at too small a heliocentric distance, indicating that the initial distance of 5.3 AU is too small. Also, the larger disk mass gives the protoplanets and Jupiter more planetesimals to scatter, and thus increases the distance they travel due to angular momentum exchange (Section 5.1).

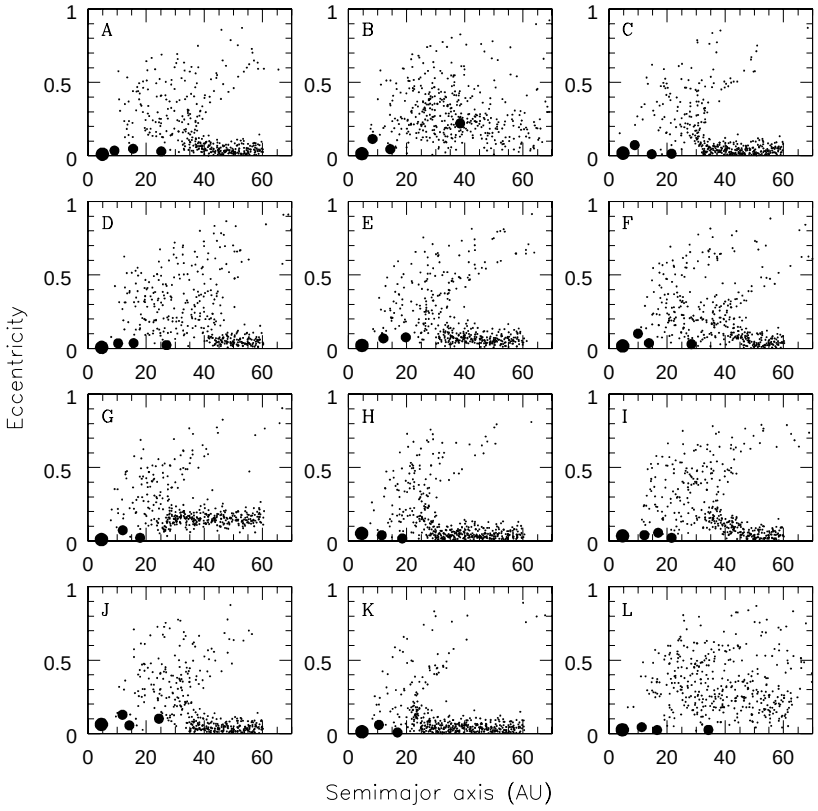

Fig. 10.— End states of the twelve Set 5 runs (a shallower disk density profile). All are run to 5×10^6 years.

5.6. Set 5: A shallower disk density profile

In this set of runs, a shallower planetesimal disk surface density, $\propto a^{-3/2}$, is used. The disk now begins at 10 AU, with the interior region being initially occupied solely by the protoplanets. In other words, it is assumed that in the epoch from which the runs start, all but a negligible mass of the planetesimals among the protoplanets has been swept up or scattered from the region. The surface density profile is given by

$$\sigma_3 = 1.8(a/10 \text{ AU})^{-3/2} \, g/cm^2 \tag{11}$$

and thus a total mass of 123 $M_\oplus$ is contained in the disk between 10 and 60 AU. Extending this planetesimal disk inward to 5 AU would yield a surface density there of only 5 g/cm^2, and a total mass between 5 and 10 AU of only 25 $M_\oplus$. Despite this, we still put four 15 $M_\oplus$ in this region; thus, it is assumed that the original planetesimal surface density profile in this region was steeper, perhaps due in part to redistribution of water vapor from other parts of the disk to the vicinity of the snow line (Stevenson & Lunine 1988).

This set consists of twelve runs, each to 5 Myrs. As before, the inner body's mass is increased to 314 $M_\oplus$ over the first 10^5 years of simulation time. The endstates are shown in Fig. 10. Eight out of twelve runs possess the right number and ordering of bodies. Eccentricities of the protoplanets and Jupiter are $\lesssim$ 0.1 in five of these. This "success rate" is close to that of Set 1 (which has a similar total disk mass); this model thus does not appear to be highly sensitive to changes in density profile alone.

Various degrees of disruption of the planetesimal disk can again be seen. Most show a sharp transition between a disrupted region crossed by the scattered planetesimals, and a largely undisturbed outer region. In Run 5A, for example, this transition occurs at slightly below 40AU, while in Run 5F, it is located between 45 and 50 AU. Runs 5B and 5L show strong disruption throughout the entire disk, indicating that all of it was crossed by one

or more protoplanets. Another state can be seen in Run 5G, where all eccentricities in the outer part of the belt are uniformly raised. This occurs when a protoplanet crosses the outer disk with an inclination high enough that it spends most of its orbit above or below, rather than inside, the disk. The disk planetesimals are then excited primarily by long-range secular effects rather than by short-range scattering encounters (TDL99). Another (less dramatic) example of this effect can be seen in Run 1G above.

5.7. Set 6: A minimum-mass disk

How well does the model work in a "minimum-mass" planetesimal disk, with a surface density as given by Eq. 1? Such a disk only contains about 13 $M_\oplus$ in solids between 5 and 10 AU. This is inconsistent with the assertion that the Jupiter-Saturn region is the source of all the giant planets, unless one invokes a very large density enhancement in that area. Nevertheless, it is useful to investigate how effective dynamical friction is in this extreme case. We repeat the baseline run (Set 1, Section 5.2), but with a planetesimal disk of the surface density given by Eq. 1. All eight runs are stopped after 10 Myrs. The endstates are shown in Fig. 11. In only two of the eight runs—6D and 6G—are all protoplanets retained. However, only in 6G are all the protoplanets noncrossing by 10 Myrs. One may conclude that the circularization of scattered protoplanets is marginally effective even in a minimum-mass disk. Therefore, this model places a stronger lower limit on the disk mass in the Jupiter-Saturn region, than in the trans-Saturnian region.

5.8. Set 7: The role of Saturn

Thus far, the only gas giant in the simulations has been Jupiter. The innermost of the scattered protoplanets does tend to end up near the present location of Saturn. However,

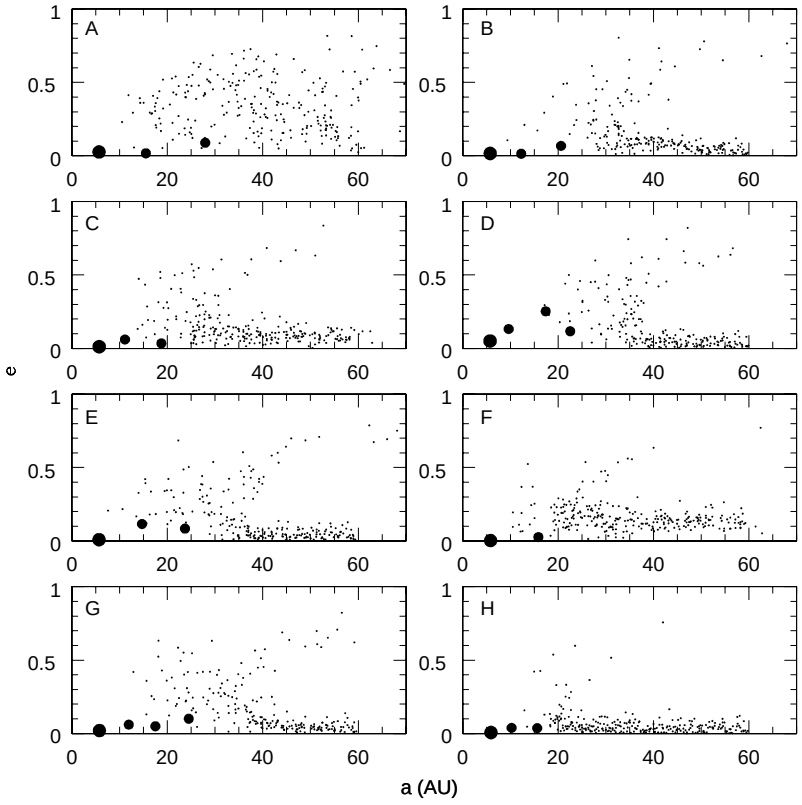

Fig. 11.— End states of the eight runs in Set 6, with a minimum-mass initial planetesimal disk. All are run to 10 Myrs

to reproduce the Solar System, it must at some point accrete ~ 80 $M_\oplus$ of nebular gas. We therefore investigate what effect the subsequent growth of a Saturn-mass object has on our model.

A Set 1 run which produced a good Solar System analogue (1F; Fig. 4) is used as a starting point. At about 1 Myr, the protoplanets and Jupiter are no longer on crossing orbits. At this time, the initially outermost protoplanet (plotted in blue) has become the innermost one, closest to Jupiter at ~ 10 AU. We perform a set of five runs which branch off from this point. In these runs, the innermost protoplanet has its mass increased to that of Saturn over a 10^5 year interval, starting at 1, 1.2, 1.4, 1.5 and 1.6 Myrs, respectively. We choose to start only after the protoplanets are on noncrossing orbits in order to avoid ending up with an eccentric "Saturn"; the eccentricity evolution of an initially eccentric giant planet in a gas disk is uncertain (Lin et al 2000).

The endstates are shown in Fig. 12. No protoplanets have been lost from the system by the end of the runs. A protoplanet still has a high eccentricity in the 1 Myr case; this is because this protoplanet's perihelion is still very close to the innermost protoplanet's orbit at 1 Myr, and it suffers strong perturbations as the latter grows to Saturn's mass. In the other cases, however, Saturn's formation does not cause large eccentricities in the protoplanets. This is as one would expect; at its final mass, and at 10 AU, Saturn's Hill radius is 0.45 AU, and by 1.2×10^6 years, the closest protoplanet's perihelion is at ~ 14 AU, almost $9\,r_H$ away, thus unlikely to be in reach of strong scattering. We leave for future work the effect of Saturn's gas accretion on systems with more protoplanets, such as those in Set 3 in Section 5.4 above. Such systems tend to have weaker stability, and thus may be more susceptible to disruption by Saturn's final growth spurt.

One effect visible in Fig. 12 is that the semimajor axis of Saturn at 5 Myrs tends to be smaller than that of the innermost scattered protoplanet—the putative proto-Saturn—in

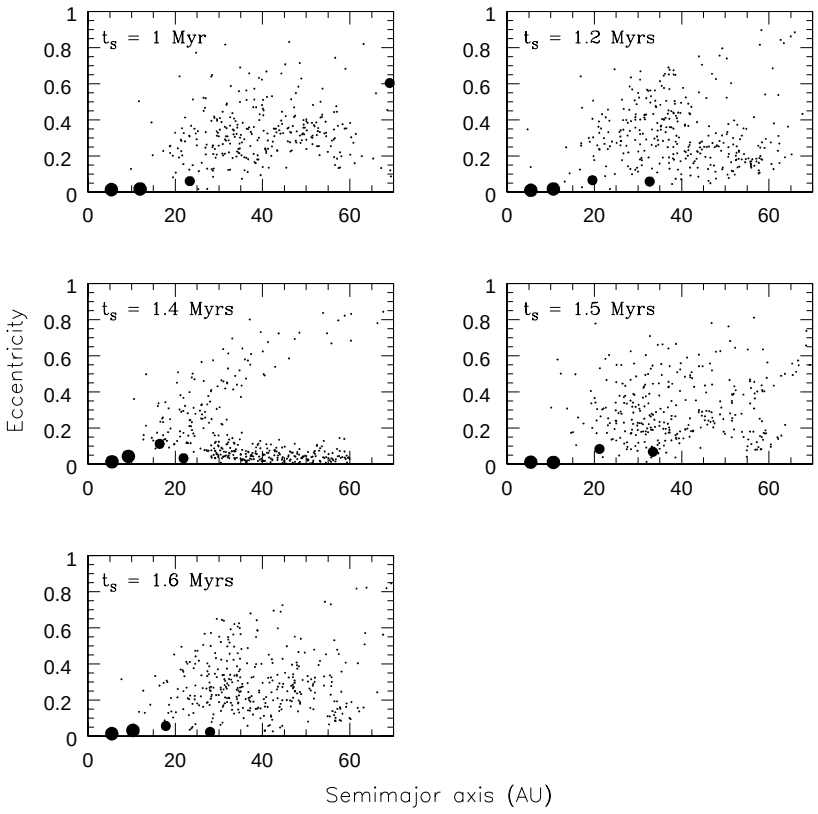

Fig. 12.— Endstates of the Set 7 runs, in which "Saturn" commences growing after the protoplanets have largely decoupled from each other. In each case, Saturn is the second-innermost of the largest points, the innermost being Jupiter. The start time of Saturn's growth, t_S, is denoted on each panel.

those runs where the gas accretion of Saturn is not modeled (see for example Fig. 6). When a protoplanet grows to Saturn's mass, its subsequent migration speed is much slower, since the rate of migration depends on how much mass in planetesimals it scatters relative to its own mass. This counteracts the tendency of the innermost scattered protoplanet to end up at a semimajor axis larger than that of present-day Saturn in the other runs, where only Jupiter grows.

6. Scattered protoplanets and the small body belts

The simulations presented above show that scattering of giant planet core-sized protoplanets is a violent event, which leaves a strong dynamical signature on the surrounding planetesimal disk. The asteroid belt and the Kuiper belt are therefore the natural places to look for evidence of large scattering events in the Solar System's early history.

6.1. The asteroid belt

It is those members of the asteroid belt larger than about 50 km in diameter which are of interest in inferring properties of the early Solar System; smaller bodies cannot be primordial because they could not have survived intact for the age of the Solar System (eg. Petit, Morbidelli and Valsecchi 1999). This population displays a high degree of dynamical excitation and a severe mass depletion, containing at most a thousanth of its orignal mass, as extrapolated from the terrestrial region (Weidenschilling 1977).

In the context of the model presented here for the early evolution of Uranus and Neptune, the initial violent scattering of protoplanets is perhaps the most obvious candidate to look to for perturbation of the asteroid belt. Indeed, in numerous runs, protoplanets

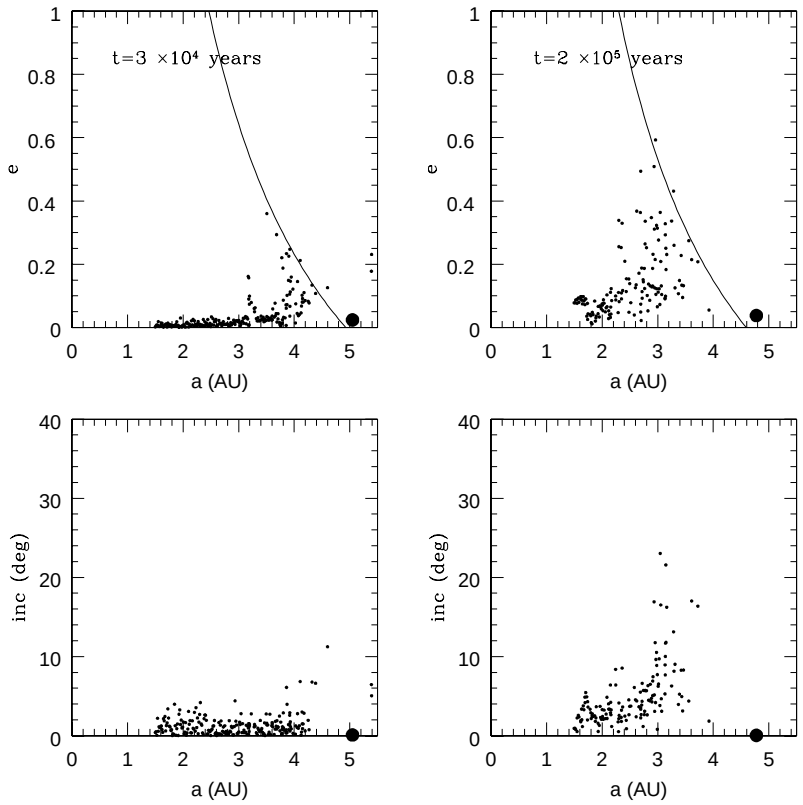

Fig. 13.— Eccentricities and inclinations of planetesimals in the asteroid belt region, interior to Jupiter (the large dot), at 3×10^4 years (top panel) and 2×10^5 years (bottom panel). These times are, respectively, just before and just after the period during which a protoplanet repeatedly crossed the region interior to Jupiter. Jupiter in this run has moved inward to $\sim$ 4.8 AU, 0.4 AU less than its present semimajor axis. The curve marks the locus of Jupiter-crossing orbits

spend some time interior to the orbit of Jupiter, crossing part of the asteroid belt region for up to $\sim 10^4$ years at a time. One might expect that such an occurence would wreak havoc in the the asteroid belt. This is analogous to the model investigated by Petit, Morbidelli and Valsecchi (1999), in which 1 $M_\oplus$ bodies are scattered by Jupiter to cross the Kuiper belt; the difference is that the bodies here are a factor of ten more massive.

To assess the effect of scattered Uranus/Neptune-sized bodies on the asteroid belt, we perform six additional runs with planetesimals added in the asteroid belt region. The individual bodies have a mass of $0.024\,M_\oplus$, and are distributed with a surface density of

$$\sigma_{belt} = 8.0(a/1\ \mathrm{AU})^{-1}\,g/cm^2 \tag{12}$$

between 2.5 and $4.5\,AU$. This shallow density profile is the same as the one used by Chambers and Wetherill (1998) in the terrestrial region, which in turn was chosen to be more consistent with the large densities required at larger heliocentric distances to form Jupiter and Saturn. The protoplanet masses in this case are $15\,M_\oplus$. We find that eccentricities can get excited to their present values in this way, though only down to the crossing protoplanet's minimum perihelion distance, which in none of the runs performed reaches the inner edge of the belt. Inclinations fare more poorly; protoplanets seldom raise them much above 10°, which is less than the present median inclination of asteroids beyond 2.5 AU. Also, very little mass is scattered out of the belt while the protoplanets are crossing it. Fig. 13 shows "before and after" snapshots of the run which, out of the six, displays the strongest disruption of the region interior to Jupiter by scattered protoplanets. As can be seen, few bodies, apart from those that are nearly Jupiter-crossing, attain inclinations above 15°. Thus despite the much more massive Jupiter-scattered bodies, our result is similar to that of Petit, Morbidelli and Valsecchi (1999): the bodies cross too little of the asteroid belt, and for too short a time, to reproduce the observed high inclinations and mass depletion.

The scattered giant protoplanet model may have figured more indirectly in the dynamical sculpting the asteroid belt region. If proto-Saturn was very close to Jupiter when it accreted its massive gas envelope—a situation favored by an initially compact region of giant planet formation—then the subsequent migration of the gas giants may have been enough to sweep the inclination-exciting ν_{16} secular resonance through most of the asteroid belt (cf. Gomes 1997, Levison et al 2001). Gomes initially places Jupiter and Saturn at 5.4 AU and 8.7 AU, respectively, which positions the ν_16 resonance at 2.7 AU. As the gas giants migrate away from each other the resonance sweeps inward, reaching 2 AU when they reach their present orbits. If Saturn were to complete its growth even closer to Jupiter, the ν_{16} resonance would start at a larger heliocentric distance, and more of the asteroid belt would be swept during the subsequent migration.

If large (lunar to martian sized) protoplanets originally accreted in the asteroid belt, then there is little or no need for any exterior sources of the belt's excitation and mass depletion; Petit, Morbidelli and Chambers (2001) show that in this case both can be well reproduced. In their simulations, protoplanets in the belt scatter the surrounding small bodies, and are eventually themselves removed through mutual scattering and perturbation by Jupiter. In this scenario, a limited role may still have been played by Jupiter-scattered bodies in the outer part of the asteroid belt, where Jupiter's influence would have impeded the formation of belt protoplanets.

6.2. The Kuiper belt

In the present Solar System, a new class of Kuiper belt object (KBO) has recently been identified (Duncan and Levison 1997, Luu et al 1997). These objects have semimajor axes and eccentricities such that they lie near the locus of Neptune-encountering objects shown in Fig. 2. They are thought to be part of a population referred to collectively as

the scattered disk—formerly low-eccentricity KBOs which have had their orbits changed by close encounters with Neptune. Many of the simulations in Section 5 show an analogous class of planetesimals in their "Kuiper belt" regions. However, these fall on the locus of orbits crossing not the final semimajor axis of the outermost protoplanet, but the furthest aphelion distance of any of the protoplanets during their initial high-eccentricity phase. Since these orbits are no longer being crossed by a protoplanet, they will be stable over long times. One can refer to these structures as "fossilized" scattered disks (TDL99), because they preserve part of the dynamical history of the planetesimal disk. Such structures only appear in runs where the initial scattering was strong enough that one or more protoplanets had their aphelia increased to well beyond the final semimajor axis of the (ultimately) outermost protoplanet.

Observations of our Solar System's Kuiper belt do indeed reveal an anomalously high degree of excitation (eg. Petit, Morbidelli & Valsecchi 1999, Malhotra, Duncan & Levison 2000). The eccentricities and, to a lesser degree, inclinations of bodies in mean-motion resonances with Neptune, particularly the 2:3 resonance at 39.5 AU, can be explained by resonance sweeping during Neptune's migration, as can the paucity of objects on nonresonant orbits interior to 39 AU (Malhotra 1995). However, the high inclinations found beyond $\sim$ 41 AU in what is commonly called the "classical" Kuiper belt, cannot be explained in this way. Petit, Morbidelli and Valsecchi (1999) propose large (up to 1 $M_\oplus$) Neptune-scattered planetesimals as the mechanism which stirred and cleared the belt. But even when such bodies remain in the belt for 100 Myrs, the inclinations they raise are almost always less than 20°.

Can the excitation of the Kuiper belt be better accounted for if we are thus far only seeing the part of it that is interior to the locus of a fossilized scattered disk? The inclinations raised by a protoplanet can be directly obtained from the simulations of Section

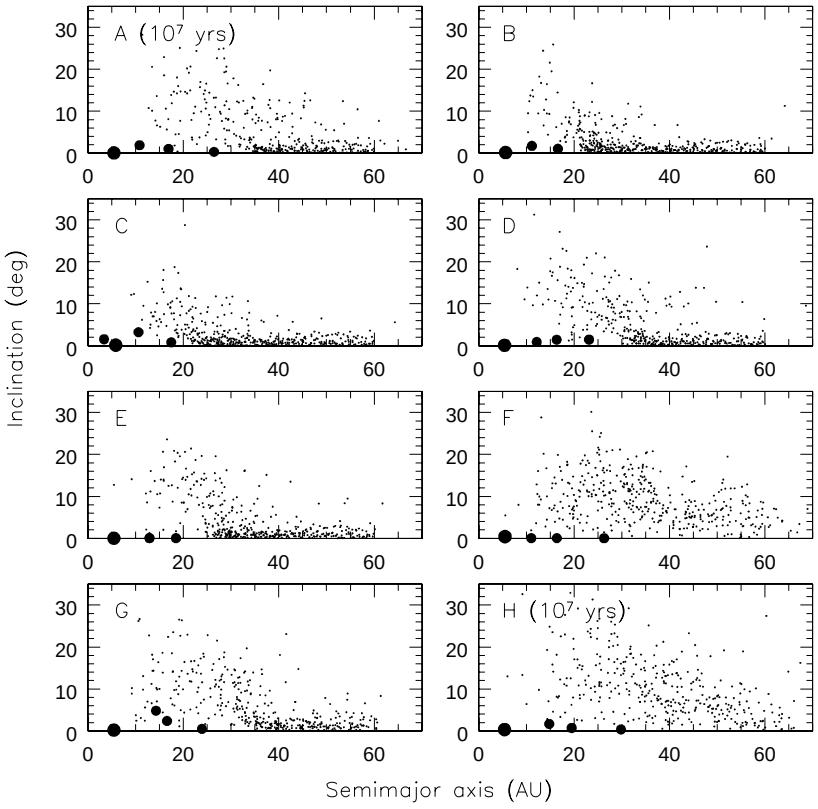

Fig. 14.— Counterpart to Fig. 6, showing inclination versus semimajor axis for the endstates of the runs in Set 1 (baseline).

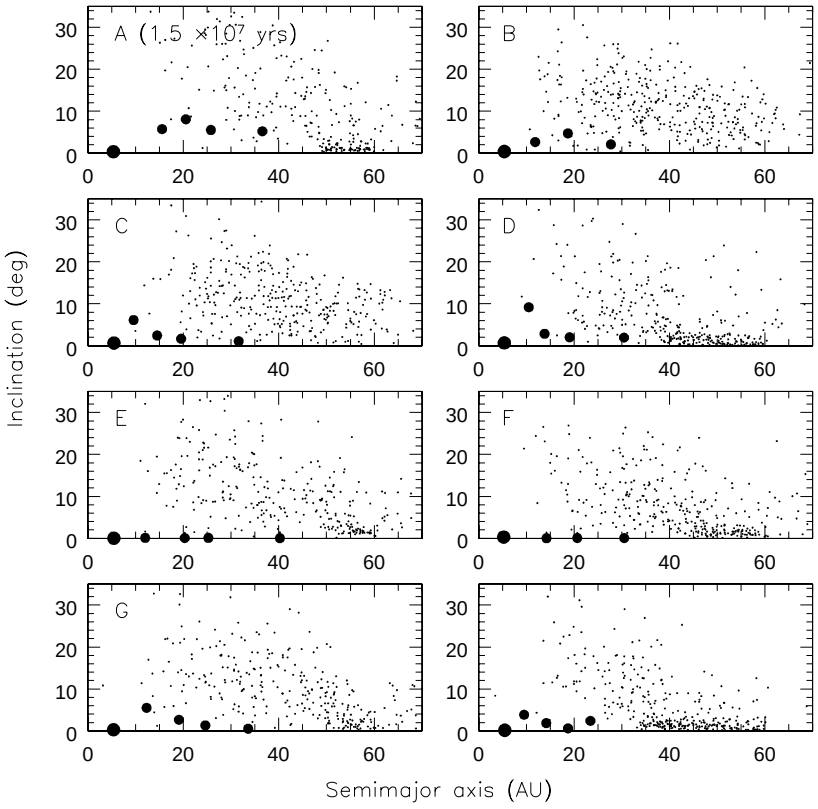

Fig. 15.— Counterpart to Fig. 8, showing inclination versus semimajor axis for the endstates of the runs in Set 3 (one extra protoplanet).

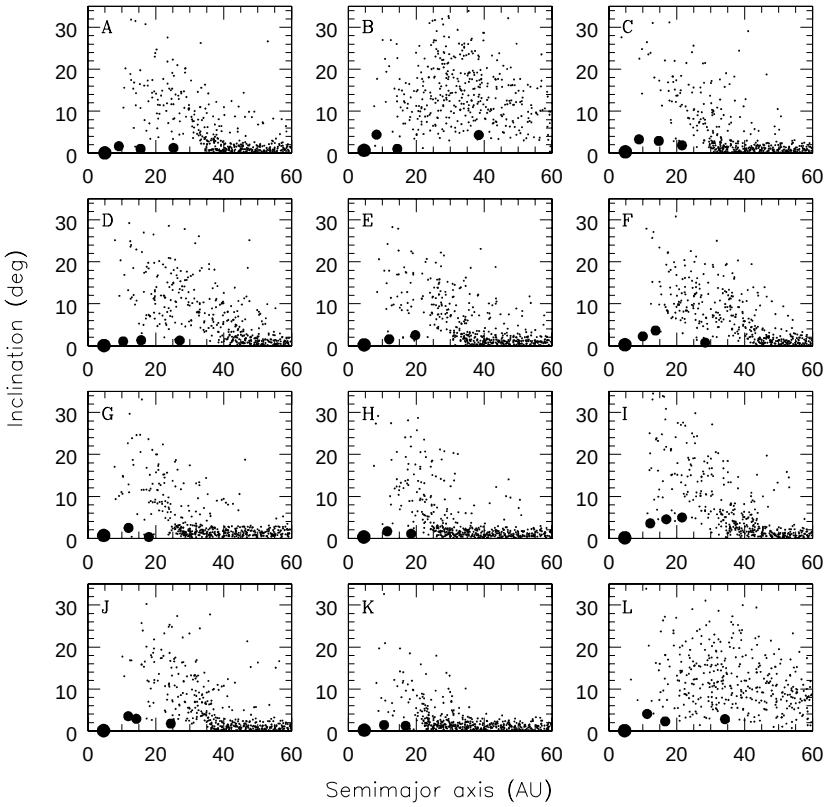

Fig. 16.— Counterpart to Fig. 10, showing inclination versus semimajor axis for the end-states of the runs in Set 5 (shallower disk density profile).

5. The runs of Set 1, Set 3 and Set 5 will be used for comparison. Their inclinations are shown in Figs. 14, 15 and 16, respectively. Inclinations beyond the outermost protoplanet are excited up to a maximum of about 30°, similar to those observed in the classical Kuiper belt today (see Fig. 2) However, observations of the Kuiper belt are biased against high-inclination objects. Brown (2001) derives a de-biased inclination distribution function for the classical belt:

$$f_t(i) = \sin(i) \left[a \exp\left(\frac{-i^2}{2\sigma_1^2}\right) + (1-a) \exp\left(\frac{-i^2}{2\sigma_2^2}\right) \right] \tag{13}$$

with $a = 0.93 \pm 0.02$, $\sigma_1 = 2.2 \pm .^2_6$, and $\sigma_2 = 17 \pm 3$. One can define a parameter $i' \equiv \cos^{-1}(\overline{\cos(i)})$ to give a measure of the characteristic inclination of a population. For the de-biased distribution above, $i' = 21°$. However, in the runs presented here, the largest i' in the region corresponding to the classical belt (between the outermost planet's 2:3 and 1:2 mean-motion resonance) is only 15°. Thus, although higher inclinations are produced here than in the large Neptune-scattered planetesimals model of Petit, Morbidelli and Valsecchi (1999), the inferred full velocity distribution of the classical Kuiper belt still cannot be accounted for.

It is possible to estimate with a simple numerical experiment if a planet as large as Uranus or Neptune can in principal excite the Kuiper belt to observed values. This experiment consists of a single Uranus-mass planet on an orbit with $a = 45AU$, $e = 0.2$, and $i = 25°$. The planet is embedded in a swarm of 400 massless test particles informally spread from 35AU to 55AU, with initial $e = 0.01$ and $i = 1°$. Fig. 17 plots the i' of the particles as a result of scattering off of the planet. It shows that a planet the mass of the ice giants can indeed excite the Kuiper belt to $i' = 20°$ in a million years.

However, in none of the runs we performed was such a high inclination imparted to a protoplanet. Alternatively, a less inclined protoplanet may be able to reproduce the Kuiper belt inclinations if it remains on a belt-crossing orbit significantly longer than 1 Myr (and

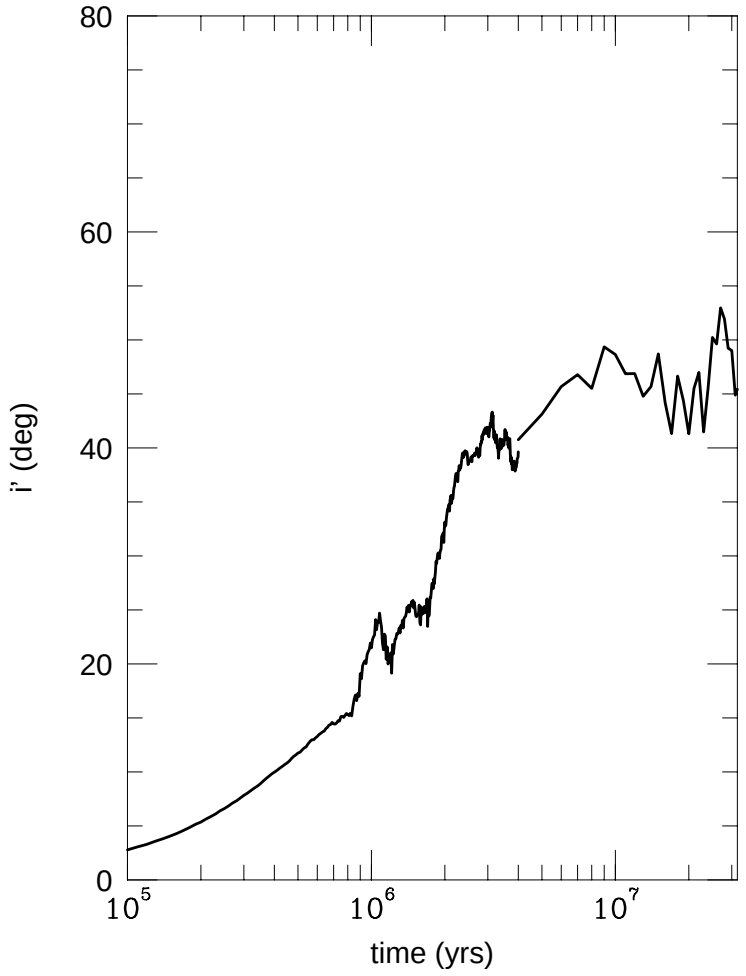

Fig. 17.— Characteristic inclination i' versus time of test particles between 35 and 55 AU, gravitationally stirred by a Uranus-mass body initially having $a = 45$ AU, $e = 0.25$, and $i = 25°$. The test particle inclinations reach the debiased value for the Kuiper belt, $i' = 20°$ (Brown 2001), after about 1 Myr.

thus longer than in our runs). Right at the outset, though, there is a caveat: If one wants to appeal to a truncation in the gas disk beyond Saturn as the mechanism which forestalls Uranus and Neptune's evolution into gas giants, then a circularization time of several million years may cause their pericenters to spend a perilously long time in the gas. In any case, one way to increase the dynamical friction timescale is by decreasing the mass of the trans-Saturnian planetesimal disk. However, this also increases the chances of protoplanets being lost altogether during scattering, and makes it more difficult to (plausibly) fit enough solids for forming all the giant planets into the Jupiter-Saturn zone (see Section 5.7). A longer circularization time will also result if a protoplanet can be decoupled from Jupiter and the other protoplanets at a larger semimajor axis. For the latter situation to have a better chance of occurring in simulations, the planetesimal disk needs to be extended to larger heliocentric distance. We will investigate this issue further in future work.

7. Discussion

The conventional picture of Uranus and Neptune's formation, whereby the ice giants accrete near their present heliocentric distances, has grave problems. Numerical simulations have not been able to produce ~ 10 $M_\oplus$ objects in the trans-Saturnian region in the lifetime of the Solar System without significantly increasing protoplanet radii, or invoking dissipational forces and planetesimal disk densities too large to be consistent with a physically plausible protostellar disk.

Building on our previous work (TDL99), we have performed additional N-body simulations of the evolution of the outer Solar System starting at the time when the first gas giant forms. At this point, we assume that a number of ~ 10 $M_\oplus$ objects have formed at a heliocentric distance of roughly 5 to 10 AU, as is suggested by the oligarchic growth model (Kokubo & Ida 1998, 2000). Using a variety of different initial conditions, we find as before

that the accretion of Jupiter's gas envelope causes the remaining protoplanets to become violently unstable. In most cases they are scattered onto high-eccentricity orbits in the trans-Saturnian region. With most of its orbit now crossing the accretionally little-evolved trans-Saturnian planetesimal disk, a scattered protoplanet experiences dynamical friction and has its eccentricity rapidly damped. As a result, the protoplanets tend to end up on nearly circular, well-spaced orbits on a timescale of a few million years, with semimajor axes comparable to those of Saturn, Uranus and Neptune. Of the simulations which initially contain a total of four giant protoplanets and form Jupiter from the innermost, the majority produce final orbital configurations similar to that of our outer Solar System. Such systems are produced—though with lower probability—even if ones adds an extra protoplanet, lets the second-innermost protoplanet grow into Jupiter, or lowers the the planetesimal disk density to the minimum-mass value. These results strengthen our earlier conclusion that if Uranus and Neptune shared the same birthplace as the gas giants, they could then readily have been delivered to their present orbits.

The role of migration in the formation of Uranus and Neptune was previously investigated numerically by Ipatov (1991), based on an idea by Zharkov and Kozenko (1990). Ipatov concludes that planetary embryos of a few $M_\oplus$ may have originated just outside the orbit of Saturn, to migrate outward and later grow into Uranus and Neptune, provided that they did not acquire high eccentricities during this process. In contrast, we find that Uranus and Neptune could have originated from anywhere in the Jupiter-Saturn region, and that initially high eccentricities—which nearby bodies naturally tend to acquire during Jupiter's final growth phase—are in fact a powerful mechanism for rapidly transporting them outward. Also, the long growth timescales in the outer Solar System suggest that Uranus and Neptune likely already completed most of their growth in the Jupiter-Saturn region; even with a "head start" of a few Earth masses, the formation of Uranus- and Neptune-mass objects much beyond 10 AU within the age of the Solar System

is unlikely (Levison and Stewart 2001, Thommes, Duncan and Levison 2002)

Can one find any observational support for this model in the present-day Solar System? The high inclinations in the classical Kuiper belt point to strong dynamical excitation in the past, and the simulations performed here do produce high inclinations in this region as a natural side effect. However, the simulations all fall short of reproducing the mean debiased inclination of the classical Kuiper belt. Strong observational support would be provided by the discovery of a fossilized scattered disk in the Kuiper belt, and a dynamically colder population beyond. It is tempting to link the trans-Neptunian object 2000 CR_{105} with a fossilized scattered disk; its high eccentricity (0.8) is characteristic of a scattered disk object, but recent observations (Gladman et al 2001) have established that its perihelion is at 44 AU, far beyond the reach of Neptune. However, none of the fossilized disk objects in our simulations acquire semimajor axes as high as that of 2000 CR_{105} (216 AU). Fig. 18 shows a plot of perihelion distance versus semimajor axis for Set 5, revealing only one case (B) where one or more objects simultaneously acquire a semimajor axis of $\sim$ 100 AU and a perihelion distance significantly further out than the (circularized) outermost protoplanet. All other sets of runs fare even more poorly. 5B is a run in which a protoplanet spends a long time at high eccentricity, and excites particularly high planetesimal inclinations in the disk. A long circularization time may thus be an important ingredient in reproducing both objects like 2000 CR_{105} and the high inclinations of the Kuiper belt; we will address this possibility in future work.

Findings regarding the deuterium to hydrogen (D/H) ratios of Uranus, Neptune and comets are particularly interesting in the context of this model. From infrared observations, Feuchtgruber et al (1999) find that the D/H ratios of the ice giants are lower than those of the Oort cloud comets Halley (Eberhardt et al 1995), Hyakutake (Bockelée-Morvan et al. 1998) and Hale-Bopp (Meier et al 1998) by a factor of approximately three, a difference

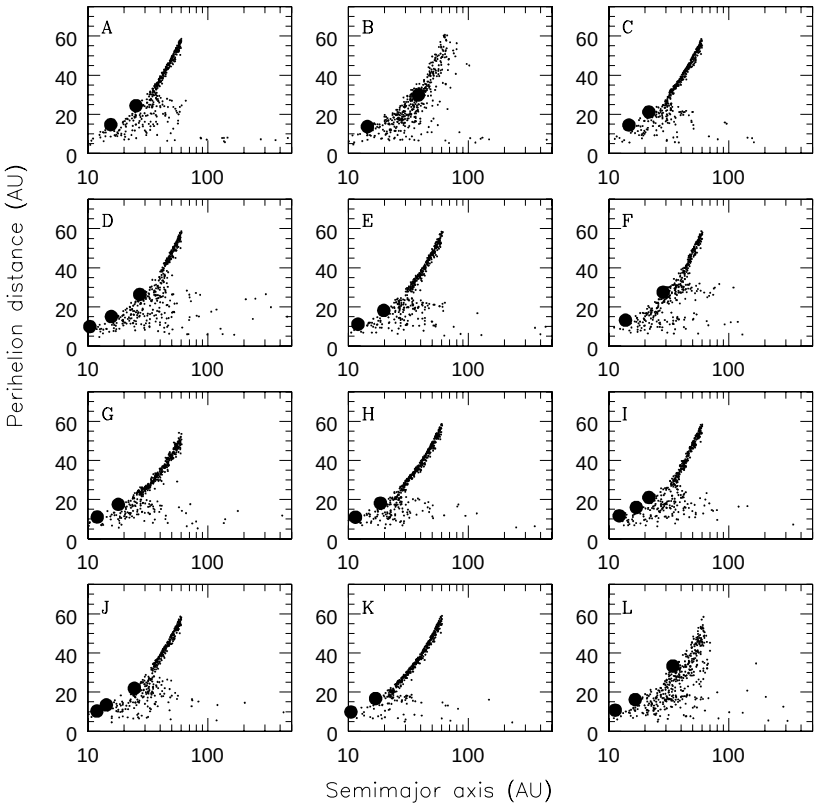

Fig. 18.— Endstates of the Set 5 runs, showing perihelion distance versus semimajor axis.

large compared to the uncertainties of the measurements. Oort cloud comets are thought to have originated primarily in what is today the Uranus-Neptune region (Duncan, Quinn & Tremaine 1987, Fernandez 1997), and the notion of a common birthplace is supported by the comets' similar D/H ratios. Though a sample size of three is clearly very small, this discrepancy between the comets and the ice giants would seem to present a further problem for any scenario in which Uranus and Neptune form in the trans-Saturnian region, since they should then share the chemical composition of the comets. However, this is exactly what one would expect if the ice giants originally formed at a smaller heliocentric distance, where higher temperatures would have made for a lower D/H ratio.

An aspect not modeled in any of the simulations is the gravitational interaction of the bodies with a gaseous disk. It has been shown that gas disk tidal forces can cause rapid inward migration of protoplanets (eg. Ward 1997). In fact, the speed of migration may be peaked for objects of ~ 10 $M_\oplus$, taking place on timescales of 10^5 years or less. This peak corresponds to the transition between so-called Type I migration, where a body's resonant interaction with the gas disk gives rise to a torque imbalance, to Type II migration, where the object opens a gap in the gas disk and is subequently locked to the disk's viscous evolution. Tidal migration therefore poses a problem for *any* model of giant planet formation: how do they avoid spiralling into the central star as they form? Perhaps gap opening already begins to take place for masses significantly smaller than 10 $M_\oplus$. In the accretion disk model of Gammie (1996), the disk is essentially inviscid beyond ~ 0.1 AU. This would lower the gap-opening threshold, though only to where the protoplanet's Hill radius is comparable to the gas disk scale height (eg. Bryden et al 2000b); the disk would thus also have to be very thin (i.e. cold). Another possibility is that the disk is truncated early on by photoevaporation from the central star (Shu, Johnstone and Hollenbach 1993), or from surrounding stars, as is seen in the Orion Nebula proplyds (Johnstone, Hollenbach and Bally 1998). Bodies scattered beyond the truncation distance would then be safe from

nebula tides, and those near the edge would experience a net positive torque and migrate outward. Of course, such a scenario has the added advantage that, as discussed in the above works, it very neatly accounts for Uranus and Neptune having no massive gas envelopes.

In constructing the simulations presented here, we have appealed to the oligarchic growth model as a plausible guide for our choice of initial protoplanet masses and orbits. One can of course envision a number of variations. For instance, two gas giants may form on initially widely separated orbits. The waves they raise in the disk will tend to clear the gas between them, and Type II migration will cause their orbital separation to decrease (Kley 2000). If ice giant sized bodies are trapped in between, they will be prevented from accreting more gas, and will be scattered as the stable region between the gas giants shrinks to nothing. Also, if future measurements of Jupiter constrain its core to be much smaller, or even absent, this will invalidate the assumption that Jupiter grew from an ice giant sized nucleus...unless the core as we detect it today is not primordial (Guillot 2001) . Though the scattering of ice giants could still take place in principal even if Jupiter did not start out as one of them, one would then need to explain how a small body won the gas accretion race against much larger bodies (if the core is small), or how ice giant sized bodies managed to form before the birth of the first gas giant from an unnucleated disk instability (if there is no core; eg. Boss 2000). Alternatively, one could search for a way in which accretion could continue to take place in close proximity to a gas giant, with scattering delayed until ice giant sized bodies form. For such a scenario Type I tidal effects, which cause the eccentricity to decay on an even shorter timescale than the semimajor axis (eg. Papaloizou & Larwood 2000), may actually be helpful. It may then be the dispersal of the gas which triggers scattering. Doing away with any reference to a specific formation process, the most general statement of our results is: *Ice giant sized bodies can be scattered from the Jupiter-Saturn region by gas giant sized bodies, to ultimately end up on Uranus- and Neptune-like orbits.*

EWT is grateful for support from the Center for Integrative Planetary Science, as well as from the National Sciences and Engineering Research Council (NSERC) during the earlier part of this work. MJD is grateful for support from NSERC. HFL is grateful for support from NASA's *Planetary Geology & Geophysics*, *Origins of Solar Systems*, and *Exobiology* programs. We would like to thank the referee, Shigeru Ida, for valuable suggestions which allowed us to improve the paper.

REFERENCES

Adachi, I., Hayashi, C. & Nakazawa, K. 1976, Prog. Theor. Phys., 56, 1756

Binney, J. & Tremain, S. 1987, Galactic Dynamics (Princeton:Princeton University Press)

Bockelee-Morvan, D. et al. 1998, Icarus, 133, 147

Borderies, N. & Goldreich, P. 1984, Celestial Mechanics, 32, 127

Brown, M. E. 2001, AJ, 121, 2804

Brunini, A. & Fernandez, J. A. 1999, P&SS, 47, 591

Brunini, A. 2000, The Transneptunian Population, 24th meeting of the IAU, Joint Discussion 4, August 2000, Manchester, England., 4, E7

Bryden, G., Lin, D. N. C., & Ida, S. 2000, ApJ, 544, 481

Bryden, G., Różyczka, M., Lin, D. N. C., & Bodenheimer, P. 2000b, ApJ, 540, 1091

Chambers, J. E. & Wetherill, G. W. 1998, Icarus, 136, 304

Chambers, J. E. 1999, in BAAS, 31, No. 4, 33.08

Chiang, E. I. & Brown, M. E. 1999, AJ, 118, 1411

Duncan, M. J., Levison, H. F. & Budd, S. M. 1995, AJ, 110, 3073.

Duncan, M., Quinn, T., & Tremaine, S. 1987, AJ, 94, 1330

Duncan, M. J. & Levison, H. F. 1997, Science, 276, 1670

Duncan, M. J., Levison, H. F. & Lee, M.-H. 1998, AJ, 116, 2067

Eberhardt, P., Reber, M., Krankowsky, D., & Hodges, R. R. 1995, A&A, 302, 301

Fernandez, J. A & Ip, W.-H. 1996, P&SS, 44, 431

Fernandez, J. A. 1997, Icarus, 129, 106

Feuchtgruber, H., Lellouch, E., Bézard, B., Encrenaz, T., de Graauw, T., & Davis, G. R. 1999, A&A, 341, L17

Gladman, B. et al 2001, preprint (astro-ph/0103435)

Gomes, R. S. 1997, AJ, 114, 396

Guillot, T. 1999, Science, 286, 72

Guillot, T. 2001, AAS/Division for Planetary Sciences Meeting, 33, 2306

Hahn, J. M. & Malhotra, R. 1999, AJ, 117, 3041

Hayashi, C. 1981, Progress of Theoretical Physics Supplement, 70, 35

Ida, S. & Makino, J. 1993, Icarus, 106, 210

Johnstone, D., Hollenbach, D., & Bally, J. 1998, ApJ, 499, 758

Kley, W. 2000, MNRAS, 313, L47

Kokubo, E. & Ida, S. 1992, PASJ, 44, 601

Kokubo, E. & Ida, S. 1996, Icarus, 123, 180

Kokubo, E. & Ida, S. 1998, Icarus, 131, 171

Kokubo, E. & Ida, S. 2000, Icarus, 143, 15

Ida, S. & Kokubo, E. 2000b, IAU Symposium, 202, E15

Ipatov, S. I. 1991, Soviet Astronomy Letters, 17, 113

Levison, H. F., Lissauer, J. J., & Duncan, M. J. 1998, AJ, 116, 1998

Levison, H. F., Dones, L., Chapman, C. R., Stern, S. A., Duncan, M. J., & Zahnle, K. 2001, Icarus, 151, 286

Levison, H. F. & Stewart, G. R. 2001, Icarus, 153, 224

Lin, D. N. C., Papaloizou, J. C. B., Terquem, C., Bryden, G., & Ida, S. 2000, Protostars and Planets IV, 1111

Lissauer, J. J. 1987, Icarus, 69, 249

Luu, J., Jewitt, D., Trujillo, C. A., Hergenrother, C. W., Chen, J., & Offutt, W. B. 1997, Nature, 387, 573

Malhotra, R. 1995, AJ, 110, 420

Malhotra, R., Duncan, M. J., & Levison, H. F. 2000, Protostars and Planets IV, 1231

Meier, R. et al. 1998, Science, 279, 1707

Mizuno, H., Nakazawa, K., & Hayashi, C. 1978, Progress of Theoretical Physics, 60, 699

Opik, E. J. 1951, Proc. R. Irish Acad., vol. 54A, p. 165-199 (1951)., 165

Papaloizou, J. C. B. & Larwood, J. D. 2000, MNRAS, 315, 823

Petit, J.-M., Morbidelli, A., & Valsecchi, G. B. 1999, Icarus, 141, 367

Petit, J.-M., Morbidelli, A. & Chambers, J. E. 2001, Icaus, 153,338

Pollack, J. B., Hubickyj, O., Bodenheimer, P., Lissauer, J. J., Podolak, M., & Greenzweig, Y. 1996, Icarus, 124, 62

Shu, F. H., Johnstone, D., & Hollenbach, D. 1993, Icarus, 106, 92

Stevenson, D. J. & Lunine, J. I. 1988, Icarus, 75, 146

Stewart, G. R. & Wetherill, G. W. 1988, Icarus, 74, 542

Strom, S. E., Edwards, S., & Skrutskie, M. F. 1990, ASP Conf. Ser. 9: Cool Stars, Stellar Systems, and the Sun, 6, 275

Thommes, E. W., Duncan, M. J., & Levison, H. F. 1999, Nature, 402, 635

Thommes, E. W. 2000. On the formation of Uranus and Neptune (Ph.D. Thesis). Ontario:Queen's University at Kingston.

Thommes, E. W., Duncan, M. J. and Levison, H. F. 2002, preprint.

Ward, W. R. 1997, Icarus, 126, 261

Ward, W. R. & Hahn, J. M. 1998, AJ, 116, 489

Weidenschilling, S. J. 1977, Ap&SS, 51, 153

Weidenschilling, S. J., Spaute, D., Davis, D. R., Marzari, F., & Ohtsuki, K. 1997, Icarus, 128, 429

Weidenschilling, S. J. & Davis, D. R. 2000, Lunar and Planetary Institute Conference, 31, 1685

Wetherill, G. W. & Stewart, G. R. 1989, Icarus, 77, 330

Wetherill, G. W. 1996, Icarus, 119, 219

Wisdom, J. & Holman, M. 1991, AJ, 102, 1528

Zharkov, V. N. & Kozenko, A. V. 1990, Soviet Astronomy Letters, 16, 73

This manuscript was prepared with the AAS LaTeX macros v5.0.